Modelling the ultimate pullout resistance of geogrids

D. H. Marx[1] and J. G. Zornberg[2]

[1]*Postdoctoral Fellow, Maseeh Department of Civil, Architectural and Environmental Engineering, The University of Texas at Austin, Austin, USA, E-mail: dawie.marx@utexas.edu (corresponding author) (Orcid:0000-0002-5610-5755)*
[2]*Professor, Maseeh Department of Civil, Architectural and Environmental Engineering, The University of Texas at Austin, Austin, USA, E-mail: zornberg@mail.utexas.edu*

Received 15 November 2023, accepted 14 June 2024, first published online 25 June 2024

ABSTRACT: This paper provides a review of the modelling of geogrid ultimate pullout resistance. Several analytical models were found to disregard the effect of the geogrid stiffness as well as the particle size distribution of the soil. A sensitivity analysis was done on 289 pullout tests to evaluate the significance of these omitted variables as well as other key variables contributing to pullout resistance. It was found that ultimate pullout resistance was the most sensitive to normal stress followed by geogrid length, geogrid stiffness and the friction angle of the soil. By considering geogrid geometry, stiffness and soil grading descriptors, in addition to the standard variables of length, stress and friction angle, regression models of ultimate pullout capacity improved by 15%. In addition, an alternative model to the simplified linear models of FHWA and EBGEO which maintains dimensional consistency while incorporating geogrid stiffness and non-linearity in the model, was proposed. This alternative model performed 32% better than the simplified linear models.

KEYWORDS: Geosynthetics, Geosynthetic-reinforced soils walls & slopes, Soil-geosynthetic interaction, Regression analysis, Sensitivity analysis

REFERENCE: Marx, D. H. and Zornberg, J. G. (2025). Modelling the ultimate pullout resistance of geogrids. *Geosynthetics International*, **32**, No. 3, 355–372. [https://doi.org/10.1680/jgein.23.00172]

1. INTRODUCTION

The ultimate pullout capacity of a geogrid is a key consideration in the design of reinforced structures. Most models for ultimate pullout capacity do not consider the interaction of individual geogrid ribs with particles of soil. Instead, the behaviour of the soil-geogrid composite is considered, – for example, the interface shear strength, the pullout strength, or the coefficient of soil-geosynthetic interaction. While useful for routine design, these generalized models tend to be conservative. In addition, modelling the contribution and behaviour of the individual ribs is necessary to compare the performance of several geogrids in a given soil type or the difference in performance of a given geogrid in different soil types.

In the first section of the paper a review of geogrid pullout resistance modelling is provided. Next a sensitivity analysis is conducted to determine the key variables affecting soil-geogrid interaction. Finally, the significance of including all the key variables in pullout resistance modelling is determined using regression analysis.

2. OVERVIEW OF MODELS FOR ULTIMATE PULLOUT RESISTANCE

2.1. Development of mechanistic models for ultimate pullout resistance

The prediction of geogrid pullout capacity has been extensively investigated and modelled in the literature. A geogrid interacts with the soil body predominantly through three mechanisms: (1) bearing of the transverse ribs against the soil body, (2) frictional resistance along the surface of the geogrid, and (3) frictional resistance between the soil locked into the geogrid apertures and the surrounding soil body (Jewell *et al.* 1985). Some models consider the interaction of individual ribs with the soil – that is, the geogrid is modelled as a 'grid-like' inclusion. Other models calculate an average interaction factor across the geogrid – that is, the geogrid is considered to be a sheet.

An idealized representation of the development of models for geogrid ultimate pullout resistance is presented in Figure 1. The first mechanistic models (Jewell *et al.* 1985; Koerner *et al.* 1989) modelled the geogrid ultimate pullout resistance (P_r) as the sum of the frictional

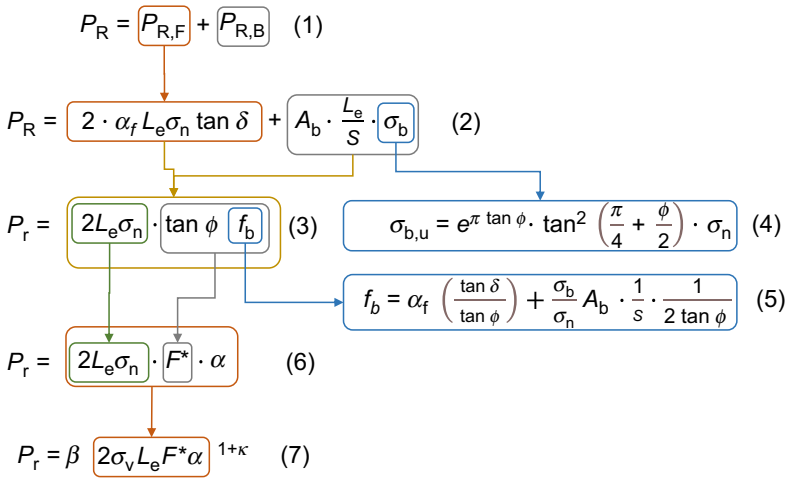

Figure 1. Development of a simplified mechanistic model for ultimate pullout resistance

resistance along the surface of the geogrid ($P_{R,F}$) and the bearing resistance of the individual transverse ribs ($P_{R,B}$) (see Equation (1), Figure 1). The frictional resistance depends on the fraction of the solid area of the geogrid (a_f), the anchorage length (L), the normal stress acting on the geogrid (σ_n) and the soil-geogrid interface friction angle (δ) (see Equation (2), Figure 1). The bearing resistance is a function of the transverse rib spacing (S_T), the bearing area of the transverse ribs (A_b) and the bearing resistance provided by each transverse rib (σ_b) (see Equation (2), Figure 1). Several solutions have been proposed to calculate the bearing resistance provided by the ribs, such as the upper bound solution by Jewell *et al.* (1985) shown in Equation (4), Figure 1. Typically, the bearing resistance is derived from bearing capacity solutions for foundations and considers the soil friction angle (ϕ) and the normal stress.

Later models merged the frictional and bearing resistance components into the product of two variables: $\tan\phi{\cdot}f_b$ (f_b is defined in Equation (5), Figure 1) (Jewell 1990). Similarly, Christopher *et al.* (1990) reduced the soil-geogrid interaction to a single 'pullout resistance factor' (F^*) (see Equation (6), Figure 1). In addition, Christopher *et al.* (1990) also modelled the non-linear stress distribution along the geogrid due to the extension of the geogrid and strain softening of the soil. This behaviour was defined in terms of the scale correction factor (α).

In practice, the soil-geogrid interaction and the non-linear stress distribution are typically lumped into a single variable $F^*\alpha$ (Huang and Bathurst 2009). This results in a simplified linear model for ultimate pullout resistance. Often, the default values prescribed by Berg *et al.* (2009) in the FHWA design manual is used: $F^* = (2/3){\cdot}\tan\phi$ and for geogrids $\alpha = 0.8$. Thus, $F^*\alpha = 0.53{\cdot}\tan\phi$. The EBGEO design manual (German Geotechnical Society 2011) prescribes a single friction factor, $f_{sg,k} = F^*\alpha$, with a comparable default value of $0.5{\cdot}\tan\phi$.

For the default values of $F^*\alpha$, the relationship between P_R, σ_n, L and $\tan\phi$ is linear in the simplified model. However, experimentally measured pullout resistance shows distinctly non-linear behaviour (Lopes and Ladeira 1996; Moraci and Recalcati 2006; Huang and Bathurst 2009; Miyata and Bathurst 2012). Thus, non-linear corrections such as the one shown in Equation (7) (Figure 1) have been proposed (Huang and Bathurst 2009; Miyata and Bathurst 2012). Furthermore, the default $F^*\alpha$ values were developed for cohesionless soils and tend to underestimate the interaction in cohesive soils (Abu-Farsakh *et al.* 2006).

2.2. Improvements to the mechanistic model

Improvements to the general model presented in Figure 1 have been developed throughout literature to better capture the complexity of soil-geogrid interaction. The following sections discuss several of these improvements.

2.2.1. *Soil particle size*

The size of the soil particles (D_{50}) relative to the geogrid apertures (A) has been reported to influence the load transfer efficiency from the geogrid to soil. In Table 1 the optimum A/D_{50} ratio reported for 13 studies is summarized. The studies are ranked based on the optimal A/D_{50} reported. For each study an overview of the test type, the soils tested, and the geogrids tested is shown. In addition, the median coefficient of curvature ($C_{z,med}$), median coefficient of uniformity ($C_{u,med}$) and median, average particle size ($D_{50,med}$) of each test is presented. The studies involved plate load testing, triaxial testing, pullout testing, shear tests and Discrete Element Modelling.

The small sample size of optimum A/D_{50}'s presented in Table 1 limits the generalization of its interpretation. Nevertheless, two trends can be observed from the data in Table 1. Firstly, two groups of optimums were measured. The first group consisted mainly of tests conducted on ballast and had a median, optimum A/D_{50} of 1.38. For the second group of tests that consisted of a wider range of soils, a median optimum A/D_{50} of 3.71 was measured.

The optimum A/D_{50} is a function of the load transfer from the soil to the geogrid, but also the load transfer within the soil itself. Relatively small geogrid apertures will inhibit load transfer from the geogrid to the soil due to a lack of interlock. Relatively large geogrid apertures will transfer load to the soil locally, rather than activating the full soil body. In granular materials load is transferred along force chains. These force chains are related to the

Table 1. Summary of 13 studies that investigated the optimum A/D_{50} for soil-geogrid interaction

Rank	Study	Test	Soils	$C_{z,med}$	$C_{u,med}$	$D_{50,med}$	Geogrid	Optimum A/D_{50}
1	Sweta and Hussaini (2018)	Direct shear, large	Granite ballast (1)	1.0	2.2	42.0	Various (5)	0.95
2	Indraratna *et al.* (2012)	Direct shear, large	Latite ballast (1)	1.1	1.9	35.0	Various (7)	1.20
3	Indraratna *et al.* (2013)	Process simulation test	Latite ballast (1)	1.1	1.9	35.0	Various (4)	1.21
4	Liu *et al.* (2021)	Direct shear, large	Latite ballast (1)	1.2	2.3	32.0	Unknown	1.35
5	McDowell *et al.* (2006)	Pullout, DEM	Ballast (1)	1.0	1.4	37.0	Biaxial (4)	1.40
6	Brown *et al.* (2007)	Composite element test	Ballast (1)	1.1	1.5	38.4	Unitized, biaxial (6)	1.41
7	Han *et al.* (2018)	Direct shear, large	Crushed limestone (3)	1.0	1.2	22.0	Unitized, various (2)	1.51
8	Miao *et al.* (2020)	Pullout, DEM	Ballast (6)	1.0	1.0	14.3	Triaxial, biaxial (1)	1.56
9	Kang *et al.* (2020)	Triaxial, large, repeated	Crushed dolomite (3)	1.6	76.5	6.5	Unitized, various (2)	3.25
10	Sarsby (1985)	Direct shear, large	Various (10)	1.0	7.1	1.0	Various (2)	3.50
11	Tavakoli Mehrjardi and Khazaei (2017)	Plate load test	Various (4)	1.0	1.7	8.4	Woven (2)	3.75
12	Wang *et al.* (2021)	Direct shear, cyclic and monotonic	Various (10)	0.9	1.3	5.9	Unitized, biaxial (1)	3.85
13	Derksen *et al.* (2022)	Biaxial Compression	Fused Quartz (1)	1.0	1.7	7.2	Biaxial, various (7)	4.20

width of the shear band that develops in the soil at large strain (Guo 2012). Some researchers found that the normalized shear band width (w/D_{50}) that develops in soil decreases with an increase in particle size (Alshibli and Sture 1999; Desrues and Viggiani 2004; Abdi and Mirzaeifar 2017). Thus, the larger ballast particles in Table 1 may develop a narrower, normalized shear band, which would correspond to a smaller optimum A/D_{50}. In contrast, other researchers have found that w/D_{50} is unique across particle sizes (Mühlhaus and Vardoulakis 1987; Oda and Kazama 1998; Rattez *et al.* 2022). Further investigation into the difference in these two families of optimum falls outside the scope of the present study.

The second trend visible in the data presented in Table 1 is that the optimum A/D_{50} was independent of the type of interaction experiment for both clusters of optimums. For a geogrid to improve the soil, whether through stabilization or reinforcement, load needs to be transferred from the soil grains to the geogrid ribs. Internally, load is transferred through the soil body along force chains. The lengths of these force chains are a function of the soil properties, rather than the method of load application. Thus, comparable optimum values of A/D_{50} were found for the different types of tests.

While an optimum A/D_{50} clearly exists, none of the 20 models for geogrid pullout resistance investigated in this study incorporates this ratio. At most, one of the models (Christopher *et al.*, 1989) states that their model is reasonably conservative for $A/D_{50} > 3$. Other attempts to incorporate particle size considers the ratio of D_{50} relative to the transverse rib thickness (t_T). For these corrections, the bearing resistance provided by a transverse rib is increased when $t_T/D_{50} < 10$ (Palmeira and Milligan 1989; Jewell 1990).

2.2.2. *Transverse rib interference*

Dyer (1985) found that when transverse ribs are spaced too closely together the regions of the soil body mobilized by successive transverse ribs overlaps. Once overlap occurs, commonly referred to as 'interference,' the load bearing capacity of a geogrid is lower than that of the sum of the resistance by the individual ribs. The effect of interference has typically been quantified as the ratio of the transverse rib spacing (S_T) to the transverse rib thickness (t_T). For $S_T/t_T < 40$, the bearing capacity of the ribs is reduced. At the extreme of $S_T/t_T \approx 0$, the geogrid is modelled as a rough sheet (Palmeira and Milligan 1989; Bergado and Chai 1994; Cardile *et al.* 2017). In addition, the friction angle of the soil has been found to influence the degree of interference (Christopher *et al.* 1989; Jewell 1990).

Following the experimental results by Milligan *et al.* (1990), Moraci and Recalcati (2006) reduced the area of the geogrid providing purely frictional resistance when the transverse ribs result in passive bearing failure of the adjacent soil. The reduction to the area only applies during residual pullout and assumes that the bearing failure extends $40 \cdot t_T$ from each rib.

2.2.3. *Transverse rib bearing resistance*

The ultimate bearing resistance (σ_b) for an individual transverse rib can be calculated using limit equilibrium. Different assumptions have been made for the governing failure mechanism. Some authors considered the ribs to behave similar to a rotated footing (Jewell *et al.* 1985; Matsui *et al.* 1996). In this case the failure mechanism is often based on the one proposed by Prandtl (1920), with differences in assumptions made for the wedge angle and the logarithmic spiral. Matsui *et al.*'s (1996) interpretation seems to fit the experimental data best. The solution by Jewell *et al.* (1985) provides an upper bound to the experimental data. Others authors considered the rib moving through the soil as similar to a punching failure (Jewell *et al.* 1985; Bergado and Chai 1994). For cohesive backfill Bergado *et al.* (1987) treated the ribs as deeply embedded strip footings.

In centrifuge testing, footings smaller than 15 particle diameters in width deviated from expected footing

behaviour (Ovesen 1979; Taylor 1995). Thus, in the case of geogrids where the transverse ribs are also small relative to the size of the soil particles, bearing capacity solutions may not accurately represent the soil geogrid interaction. As an alternative, Ziegler and Timmers (2004) assumed that the transverse ribs cut into the soil like a plough. The volume of soil mobilized by these transverse 'ploughs' provides frictional resistance against the adjacent soil body, thereby increasing the pullout resistance of the composite.

2.2.4. *Active length*

The models presented in Figure 1 assume that all transverse ribs provide the same degree of bearing resistance – that is, the distribution of the stress in the soil along the geogrid is uniform. However, experimental measurements showed that the strain in the geogrid during pullout decreased from a maximum at the front to zero at a given distance along the geogrid (Ochiai *et al*. 1996; Cardile *et al*. 2016). Thus, the resistance to pullout also decreased non-linearly along the length of the geogrid. The distance from the front of the geogrid to the point of zero extension (strain) is known as the 'active length' (L_A) of the geogrid. Cardile *et al*. (2016) used the active length to calculate an apparent coefficient of friction (μ_{AL}) for the soil-geosynthetic interface:

$$\mu_{AL} = \frac{P_R}{2L_A\sigma_n} \tag{8}$$

2.2.5. *Other factors*

Alfaro *et al*. (1995b) separated the contribution of the purely frictional resistance ('2D interaction') to pullout from the so-called '3D interaction' at the edges of the geogrid. Dilation of the soil body at the edges of the geogrid was found to be restrained by the non-dilating soil mass directly adjacent to the geogrid. In addition, the vertical dilation of the soil mobilized by the geogrid was restrained by the adjacent soil body similar to the findings by Lo (2003) for strap reinforcements. The significance of the effect was found to decrease with increasing confining stress. Similarly, the transverse ribs of a geogrid mobilizes a three-dimensional body of soil (Moraci and Recalcati 2006). This results in a local increase in the confinement applied to the geogrid. Finally, lateral expansion of the soil may be restrained by the tensile confinement provided by the geogrid apertures (Liu *et al*. 2014).

The significance of the three-dimensional dilatancy effect on soil-geogrid interaction was found to reduce with increasing confining stress (Alfaro *et al*. 1995a; Moraci and Recalcati 2006). This three-dimensional dilatancy effect is the result of complex interaction between the geogrid geometry and soil dilation. Consequently, consideration of this effect falls outside of the scope of the regression models and sensitivity analysis presented in later sections of the paper.

In reinforcement applications, geogrids are installed such that the applied load is perpendicular to the ribs that provides the greatest bearing resistance, – that is perpendicular to the transverse ribs and along the machine direction. However, in some applications the direction of load application may not necessarily be perpendicular to the orientation of the transverse ribs. For example, in the case of a three-dimensional slope stability problem, failure sliding may occur at an angle to the machine direction of the geogrid (Collin *et al*. 2021). The effect of the direction of load application on the pullout response of geogrids falls outside the scope of this study.

2.3. Alternative models

2.3.1. *Embedded sheet*

Rather than individually modelling the interaction of each geogrid rib with the soil, the geogrid can be modelled as a planar sheet embedded in the soil. The development of tensile stress along the length of the sheet can then be modelled by considering the local equilibrium along the interface:

$$\frac{dT}{dx} = -2\tau \tag{9}$$

where dT is the change in unit tension over a length dx and τ is the interface shear stress between the geosynthetic and soil.

Different assumptions have been made in the literature to solve the partial differential equation in Equation (9). Abramento and Whittle (1993) used shear lag analysis from the field of fibre reinforced composites. Other authors assumed the shear stress-displacement relationship to be elastic-perfectly plastic (Sobhi and Wu 1996), bi-linear (Madhav *et al*. 1998), hyperbolic (Gurung and Iwao 1999; Perkins and Cuelho 1999) or show strain softening behaviour (Alobaidi *et al*. 1997). Furthermore, the stress-strain response of the geosynthetic can be modelled as linear (Sobhi and Wu 1996) or hyperbolic (Perkins and Cuelho 1999). Typically, this class of models is used to calculate the pullout resistance of geotextiles embedded in soil. However, it has also been successfully applied to geogrids (Perkins and Cuelho 1999; Sugimoto and Alagiyawanna 2003; Zornberg *et al*. 2017).

2.3.2. *Calibrated incremental models*

The mechanistic models shown in Figure 1 are limited in that they do not model the development of pullout resistance with increasing displacement. Furthermore, they do not consider the extension of geogrids during pullout. Several authors developed incremental models for pullout-displacement (Palmeira 2009) to capture the dependency of the magnitude of pullout resistance on the mobilized displacements. These models share the following general form:

(1) Assume a displacement and force at the front of the geogrid.
(2) Calculate: (a) the bearing resistance mobilized at the first transverse rib due to displacement, (b) the extension of the first segment due to the applied force and (c) the frictional resistance of the first segment.
(3) Calculate the bearing resistance, extension and frictional resistance for subsequent ribs based on the extension of the prior segments.
(4) Iterate by adjusting the applied force until the force at $L = 0$ is 0.

The various incremental models differ in their assumptions regarding the development of rib bearing resistance with displacement, as well as the constitutive relationship assumed for the shear stress along the interface. For example, Bergado and Chai (1994) modelled the bearing resistance to increase hyperbolically with displacement. The relationship between shear stress and displacement was assumed to be elastic-perfectly plastic. In contrast, Sieira *et al*. (2009) modelled the bearing resistance to increase linearly with geogrid strain, and the shear-stress as hyperbolically related to displacement. Wilson-Fahmy and Koerner (1993) also considered a hyperbolic relationship between bearing resistance and displacement. However, they further distinguished between three different behaviours for the transverse ribs: stiff (rib remains straight), beam (rib deflects as either a fixed or hinged beam) and flexible (rib deflects as a parabola).

Palmeira (2004), Teixeira *et al*. (2007) and Jacobs *et al*. (2014) used the results of single transverse rib pullout tests as input for their models. In addition, the model by Teixeira *et al*. (2007) requires the experimentally measured frictional resistance of individual longitudinal ribs. Thus, a significant limitation of this group of models is that they often require coefficients calibrated using specialized laboratory tests.

2.3.3. *Machine learning*

As an alternative to the previously discussed mechanistic models, machine learning can be used to predict the ultimate geogrid pullout resistance. These models do not presume any relationship between the input variables and ultimate pullout resistance. Rather, a relationship is established by iteratively training the models on a dataset of pullout tests.

Pant and Ramana (2022) used extreme gradient boosting to predict ultimate pullout resistance using the normal stress applied (σ_n), fines content of the soil (FC), D_{50}, the embedment length (L), the ultimate strength of the geogrid (T_{Ult}) and the spacing of the longitudinal and transverse ribs (S_L, S_T) as input parameters. Limitations of machine learning models include that they are effectively a 'black box' and also should not be used outside the domain of the training data (Castelvecchi 2016).

2.4. Summary of the models

Modelling the ultimate pullout capacity of a geogrid is a complex problem as illustrated by the various alternatives proposed to the original mechanistic model by Jewell *et al*. (1985). Despite these alternatives, modelling of the intricate interaction between a soil and a geogrid remains limited. Each of the modelling approaches has their own strengths and weaknesses as summarised in Table 2. In addition, for the mechanistic models geogrid structure (t_T, S_T, S_L) is often considered but not the mechanical response (T_{Ult}, J). Furthermore, limited consideration is given to the effect of soil particle size and particle size distribution on soil-geogrid interaction for most of the models.

3. STATISTICAL EVAULATION OF VARIABLES AFFECTING PULLOUT RESISTANCE

In this section the significance of neglecting the mechanical response of the geogrid and the particle size distribution of the soil in modelling ultimate pullout resistance is evaluated. A sensitivity analysis was conducted to investigate the key soil and geogrid variables affecting the ultimate pullout resistance of geogrids. This analysis assumed no prior relationship between the variables and pullout resistance. The sensitivity analysis was followed by a regression analysis to determine the significance of ignoring some of the key variables.

3.1. Description of the dataset

A dataset of 398 pullout tests was compiled from the literature and prior studies conducted at the University of Austin (Farrag and Acar 1993; Alfaro *et al*. 1995a, 1995b; Lopes and Ladeira 1996; Raju and Fannin 1998; Goodhue *et al*. 1998; Lopes and Lopes 1999; Moraci *et al*. 2002; Teixeira 2003; Abu-Farsakh *et al*. 2006; Moraci and Recalcati 2006; Sieira *et al*. 2009; Calvarano 2012;

Table 2. Comparison of the strengths and weaknesses of the different modelling techniques for ultimate pullout resistance

Model family	Strengths	Weaknesses
Mechanistic models	• Based on the mechanisms of soil-geogrid interaction. • Generalizable for different geogrid geometries and soil types.	• Does not consider the deformation of the geogrid. • The transverse rib bearing capacity is based on plasticity solutions which may not be accurate for small t_t/D_{50}.
Simplified linear model	• Derived from a mechanistic model for interaction	• Linear • Requires calibration to be accurate
Embedded sheet models	• Closed form analytical solution. • Models the pullout load-displacement curve.	• Does not explicitly consider the interaction of individual ribs with the soil.
Calibrated incremental models	• Models the pullout load-displacement curve.	• Requires specialized testing for calibration.
Machine learning models	• Accurately captures the non-linear dependency between a large number of soil and geogrid parameters. • Generalizable within the domain of the training data.	• 'Black box', – that is the interaction between input variables may not represent the actual mechanisms of soil-geogrid interaction. • Prediction is limited to the domain of the training data.

Calvarano *et al*. 2012; Zhou *et al*. 2012; Cardile *et al*. 2016; Roodi 2016; Prasad and Ramana 2016a, 2016b; Pant *et al*. 2019a, 2019b, 2019c). All tests were conducted in large pullout boxes with test conditions typically comparable to ASTM D6706-01.

Of the 398 tests, 24 tests considered the pullout resistance of the longitudinal ribs only and in 85 tests tensile failure of the geogrid occurred. Consequently, 289 tests were used in this analysis. A histogram of the measured pullout resistances for the 289 tests is shown in Figure 2. The size of the dataset analysed herein is comparable to the work done by Huang and Bathurst (2009) (318 effective values) and Pant and Ramana (2022) (220 effective values).

3.1.1. *Geogrids*

A total of 31 unique geogrids were tested in the dataset. The geogrids were manufactured from three different polymers: High Density Polyethene (HDPE), Polyethylene Terephthalate (PET) and Polypropylene (PP). The manufacturing processes included unitized, knitted and strap geogrids. Both biaxial and uniaxial geogrids were considered. Of the geogrids tested, 49% were HDPE, unitized, uniaxial geogrids, 22% were PET, knitted, uniaxial geogrids and 14% were PP, extruded, biaxial geogrids. The remaining 15% of the products consisted of various other HDPE and PET geogrids.

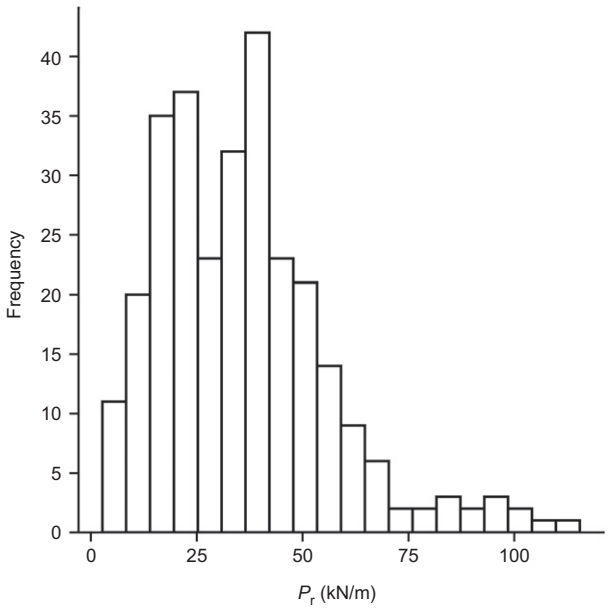

Figure 2. Distribution of ultimate pullout resistance for tests considered in this study

Based on the analytical models, and their limitations discussed in Section 2, the geogrid properties considered for the analysis were: the aperture size between the transverse and longitudinal ribs (A_T, A_L), the average transverse rib thickness (t_{avg}), the secant tensile modulus at 5% axial strain ($J_{5\%}$) and the ultimate tensile strength in the longitudinal direction (T_{Ult}). The first quartile, median and second quartile of these properties are summarised in Table 3.

Most of the tests in the dataset were conducted on new geogrid specimens. Thus, the time and temperature dependence of the tensile stiffness will not be considered. In addition, strain dependence of the tensile stiffness was not considered, as accurate strain measurements were not available for all of the products in the database. The representative value of $J_{5\%}$ was selected as it was the most commonly reported for all the tests in the dataset.

Due to homogenous manufacturing processes, specifically in the case of unitized geogrids, a strong correlation may exist between the geogrid properties (collinearity). These correlated properties were pruned to simplify modelling the relationship between ultimate the pullout resistance and the properties of the geogrid. The five geogrid properties considered in the analysis were tested for collinearity using Spearman's correlation coefficient (ρ) (Spearman 1904). Spearman's correlation coefficient is equivalent to calculating Pearson's correlation coefficient (R) (Ang and Tang 2007) on the rank of the datapoints, rather than the actual values. Consequent, Spearman's coefficient tests whether two variables monotonically increase or decrease together. This makes the coefficient robust against outliers. The resulting correlation coefficients between the geogrid properties, as well as the correlation with P_R, are summarized in Figure 3.

Some correlation was observed between the aperture sizes in the longitudinal and transverse directions. For unitized geogrids (49% of the dataset), the ratio between A_T and A_L is a function of the draw ratio in the two directions. The draw ratio represents the elongation of the base polymer sheet when it is stretched during manufacturing. This ratio dictates the creep performance, modulus and strength of a geogrid (Koerner 2012). Similar, optimized draw ratios can be expected for a given polymer across manufacturers. Consequently, A_L and A_T will be correlated across different products. The same explanation holds for the correlation between the transverse rib thickness and aperture size between transverse ribs. However, the

Table 3. Properties of the geogrids in the dataset

Quartile	Aperture size (mm)		Transverse rib thickness (t_T) (mm)	Secant tensile modulus at 5% strain ($J_{5\%}$) (kN/m)	Ultimate strength (T_{Ult}) (kN/m)
	Transverse (A_T)	Longitudinal (A_L)			
Q_1	37.9 (36.4)[a]	11.1 (16.5)	1.6 (1.4)	468 (390)	55 (60)
Q_2	70.2 (144.8)	16.5 (19.6)	2.9 (3.4)	640 (720)	80 (80)
Q_3	220 (220.0)	24.5 (27.0)	3.9 (3.9)	1041 (1098)	99 (99)

[a]Numbers in brackets refer to the statistics weighted by the number of datapoints in the dataset.

correlations were not strong enough to justify removing any of the three variables from the subsequent modelling.

The ultimate tensile strengths of the geogrids (T_{Ult}) were strongly correlated to their secant stiffnesses ($J_{5\%}$) for the geogrids considered in this dataset. T_{Ult} was assumed to be representative of the possibility a geogrid would rupture. In contrast, $J_{5\%}$ was assumed to be a better indicator of the geogrid extensibility during pullout. Thus, of the two variables, only $J_{5\%}$ was used in the subsequent analysis.

It is striking that, of the five variables considered, only $J_{5\%}$ correlated with P_R to some degree. However, $J_{5\%}$ is not considered in the mechanistic models or the simplified linear models (e.g. FHWA or EBGEO) discussed in Section 2.

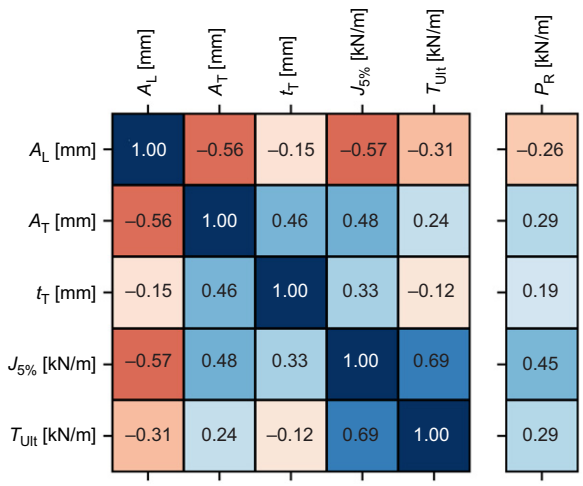

Figure 3. Pairwise correlation (Spearman) of the geogrid properties

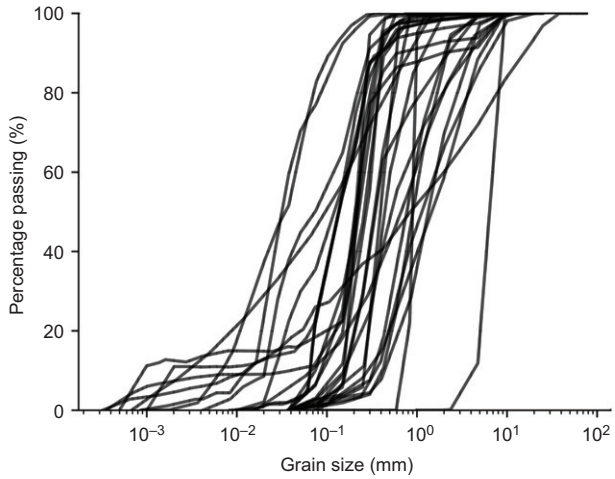

Figure 4. Particle size distributions of the soils in the dataset

3.1.2. *Soils*

Twenty-nine different soils were tested in the dataset considered. The soils consisted of conventional backfills and nonconventional materials such as coal ash, slag and foundry sands. Figure 4 presents the particle size distributions of all 29 soils. Table 4 summarizes the key soil properties considered: median particle size (D_{50}), 90th percentile particle size (D_{90}), coefficient of curvature (C_Z), fines content (percentage particles smaller than 0.075 mm, FC) and Mohr Coulomb parameters representing the soil shear strength (ϕ, c). The coefficient of uniformity (C_U) is also shown in Table 4. However, the C_u was not considered in the subsequent analysis as the parameter did not consistently reflect the behaviour of the soil. For example, C_u for a gravel with fines can have a value in excess of 100, while the median value in the dataset was 2.7. In addition, the presence of fines in the soil is already reflected in the FC parameter.

The reported soil shear strength parameters correspond to peak strength values where available. For tests conducted on dry sand and ballast, ϕ and c correspond to effective stress parameters. However, soils were tested at the optimum moisture content, – that is, under unsaturated conditions ϕ and c are best regarded as total stress shear strength parameters. For all tests, the shear strength parameters were measured under the same conditions at which the soil was prepared for the pullout testing.

There exists ambiguity in whether the c values reported in the literature represented true cohesion in the soil, or whether they were an artefact of the Mohr-Coulomb envelope being a linear approximation of the true non-linear failure envelope of the soils. As such c was not considered in the subsequent analysis. The consequence is that some ϕ's in the dataset were calculated as a best fit line and some ϕ's were calculated with a zero intercept.

The compactive effort used to prepare the specimens was reported in terms of either relative density (28% of tests) or percentage of the Maximum Dry Density (MDD) from one of the variations of the Proctor compaction test (72% of tests). Most tests were compacted within 95% of the respective maximum density (whether relative density or MDD). Thus, it was deemed viable to combine the different tests into a single dataset.

As with the geogrid properties, the soil properties were tested for collinearity. The Spearman correlation coefficients are shown in Figure 5. They reveal a strong

Table 4. Properties of the soils in the dataset

Quartile	FC (%)	D_{50} (mm)	D_{90} (mm)	C_u	C_c	ϕ (°)	c' (kPa)
Q_1	1.1 (0.9)[a]	0.16 (0.32)	0.40 (0.59)	2.5 (2.3)	0.96 (0.88)	36 (41)	0 (0.9)
Q_2	4.7 (1.0)	0.31 (0.35)	0.72 (0.73)	3.15 (2.7)	1.0 (0.97)	42 (41)	1 (0.9)
Q_3	22.0 (6.6)	0.84 (0.89)	2.4 (4.1)	6.6 (7.4)	1.3 (1.2)	44 (45)	9 (1.0)

[a]Numbers in brackets refer to the statistics weighted by the number of datapoints in the dataset.

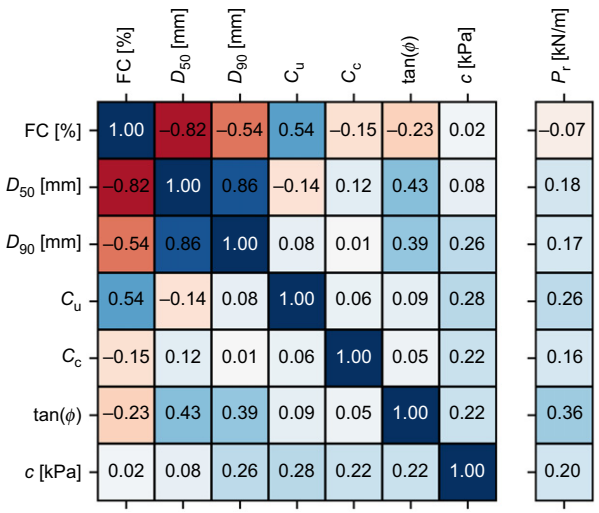

Figure 5. Pairwise correlation (Spearman) of the soil properties

correlation between the particle size descriptors D_{50} and FC as well as D_{50} and D_{90}. Consequently, only FC and D_{50} were considered in the subsequent analysis. The former property was selected to distinguish between cohesive and granular soils and the latter variable to represent the average particle size. In addition, some correlation was observed between the friction angle (ϕ) and representative particle sizes considered, D_{50} and D_{90}. However, the correlation was not significant enough to justify removing any of the properties from consideration.

3.2. Sensitivity of ultimate pullout resistance to test variables

The sensitivity of a function y in terms of a variable x, often defined as $\mathrm{d}y/\mathrm{d}x$, represents the local change in y for a local change in x, – that is the *local sensitivity*. A more relevant assessment for a non-linear problem, such as pullout resistance, is to evaluate how y varies over the domain of x, – that is the *global sensitivity* (Saltelli *et al.* 2007; Santner *et al.* 2018).

Global sensitivity analysis can be conducted using variance-based methods. The first-order effect, S_i, of the ultimate pullout resistance to a variable x_i, with distribution X_i is defined as:

$$S_i = \frac{V_i}{V(P_\mathrm{R})} = \frac{\mathrm{Var}[E(P_\mathrm{R}|X_i)]}{\mathrm{Var}(P_\mathrm{R})} \tag{10}$$

where $\mathrm{Var}(\cdot)$ and $E(\cdot)$ are the variance and expected value, respectively. Thus, the first-order effect is how much P_R varies with X_i if all other variables remain fixed. The concept can also be extended to evaluate the sensitivity of P_R to the interaction of two or more variables (second order effects).

3.2.1. *Surrogate model to smooth the ultimate pullout resistance data*

The 289 datapoints in the present study were too noisy to be used as an input for a global sensitivity analysis. Consequently, the data was first smoothed using a surrogate model. Surrogate modelling is a technique used to approximate a non-linear target function, $f(x)$, as the sum of several lower-order functions (Snyman and Wilke 2018). For the most common implementation of the technique only zero order information (i.e. the function values) is required to reconstruct the relationship between non-linear, high dimensional datapoints. This allows for accurate interpolation when the target function is unknown, – for example for the interpolation of the results of non-linear Finite Element Analysis when the computational cost of re-running the analysis is too high.

A surrogate surface can be constructed as the sum of series of radial basis functions, each centred at one of the known points in the dataset:

$$f(x) \approx \sum_{j=1}^{p} w_j \phi_j\left(x, x_\mathrm{c}^j\right) \tag{11}$$

where ϕ_j are lower-order functions centred at each of the known sets of p input variables j, and w_j is the weight for ϕ_j. For this study, thin plate splines were used as basis functions: $\phi_j = r^2 \cdot \log r$, with $r = \|x - x_\mathrm{c}^j\|^2$.

The weights can be calculated such that the surrogate surface returns the input data exactly when evaluated at those points. Alternatively, the fitted surrogate surface can be smoothed at the cost of accuracy at the original data points. When the smoothing parameter (λ) is 0, the surrogate surface fits the input data exactly, while larger values of λ are associated with a greater degree of smoothing.

In this study surrogate modelling was used to smooth the geogrid pullout resistance dataset. The surrogate surface was fitted to the input data for various values of the smoothing parameter ($\lambda = 0.01$, 1, 100). As with all models used for interpolation, the accuracy of the modelling approach had to be quantified. The dataset was split into two groups: 87.5% for fitting and 12.5% for testing. To separate the training and testing data the dataset was stratified into 37 layers based on the ultimate pullout resistance. One point was randomly selected out of each layer to create a set (or fold) of points. This process was repeated until the data was divided into eight folds of ~37 points each.

The surrogate model was fitted to the data using the *SciPy* library (Virtanen *et al.* 2020) and k-fold validation. That is, seven of the folds were used to fit the data while the eighth was used to calculate the accuracy of the model. This process was repeated until each of the eight folds was used as the testing set. The average accuracy across all eight testing sets is reported as representative (unbiased) for the model. This technique is known as k-fold cross validation (Kohavi 1995).

The accuracy of the surrogate modelling approach was evaluated in terms of the ratio of the Root Mean Squared Error (RMSE) to the standard deviation (σ) of the pullout resistance. For hydrological modelling Moriasi *et al.* (2007) considers a value of $\mathrm{RMSE}/\sigma < 0.5$ to be 'very good'. In addition, the adjusted coefficient of efficiency, E_1' (Legates and McCabe 1999, 2013) and the index of agreement, d_r (Willmott *et al.* 2012) was calculated. Both E_1' and d_r measure how well the predictions follow the model, while circumventing the pitfalls of the coefficient of determination (R^2) (Birnbaum 1973; Anderson and

Shanteau 1977; Legates and McCabe 1999). E_1' ranges from $-\infty$ to 1 for a perfect model, with $E_1' \leq 0$ indicating that the model is worse than the baseline (typically the mean). d_r ranges from -1 to 1 for a perfect model.

3.2.2. *HDMR sensitivity analysis*

Li *et al*. (2010) proposed a method for a variance-based global sensitivity analysis in the case of correlated input variables (as is the case in this study). The method entails reconstructing the relationship between x and y using a random sampling High Dimensional Model Representation (HDMR). Similar to the surrogate surface in Section 3.2.1, the target function is approximated as the sum of functions (Gao *et al*. 2023):

$$y \approx f_0 + \sum_{u=1}^{n_{12n}} f_u \tag{12}$$

where f_u are the component functions of order 1, 2 to n, and n_{12n} is the total number of component functions, – that is the sum of the number of first order functions (n_1), number of second order functions (n_2) up to the number of nth order functions (n_n).

It can be shown that the variance of y is (Gao *et al*. 2023):

$$\mathrm{Var}[y] = \sum_{u=1}^{n_{12n}} \mathrm{Var}[f_u] + \sum_{u=1}^{n_{12n}} \mathrm{Cov}\left[f_u, \sum_{m \neq u} f_m\right] \tag{13}$$

That is, the variance of y is the sum of the variances of the component functions plus the covariance between each component function f_u and the sum of all other component functions except f_u.

Next the structural sensitivity (S_u^A) and correlative sensitivity (S_u^B) can be calculated for each component function f_u:

$$S_u^A = \frac{\mathrm{Var}[f_u]}{\mathrm{Var}[y]} \quad \text{and} \quad S_u^B = \frac{\sum_{u=1}^{n_{12n}} \mathrm{Cov}\left[f_u, \sum_{m \neq u} f_m\right]}{\mathrm{Var}[y]} \tag{14}$$

The structural sensitivity represents the structure of the model, while the correlative sensitivity is the fraction of variance due to the correlation between the variables. The total sensitivity for a component u, S_u, is the sum of the structural and correlative sensitivities:

$$S_u = S_u^a + S_u^b \tag{15}$$

From Equations (14) and (15) it follows that the total sensitivity equals the variance of y, normalized by the variance of y. Thus, the sum of the total sensitivities should equal 1.

The 'extended' version of HDMR (Li and Rabitz 2012; Gao *et al*. 2023) as implemented in the *SALib* Python package (Herman and Usher 2017) was used for the sensitivity analysis. The HDMR analysis was applied to the smoothed dataset for different degrees of smoothing.

3.2.3. *Results of the sensitivity analysis*

The accuracy of the surrogate modelling technique (Section 3.2.1) in representing the geogrid pullout resistance (P_R) as a function of the ten variables (A_T, A_L, t_T, $J_{5\%}$, FC, D_{50}, C_c, $\tan\phi$, L, σ_n) first had to be validated. In Table 5 the RMSE/STD, E_1' and d_r of the surrogate model is shown for different degrees of smoothing (λ). The accuracy shown is the mean value from the k-fold validation. In Figure 6a the measured (P_R) and predicted ($\hat{P}_R$) pullout resistances are compared for $\lambda = 0.01$. Figure 6b shows the distribution of the residuals ($P_R - \hat{P}_R$), or the prediction error at each point, for the same model. Figure 7 shows similar information for $\lambda = 100$.

When the smoothing is negligible ($\lambda = 0.01$), the surrogate surface is almost an exact representation of the underlying dataset. RSME/STD is significantly lower than 0.5 and E_1' and d_r approximates 1. In addition, the residuals in Figure 6b tended towards a uniform distribution. This indicates that there is only minor bias in the model for a given value of P_R. Thus, a surrogate surface can be used to accurately model the dependency of pullout resistance on the ten input variables (A_T, A_L, t_T, $J_{5\%}$, FC, D_{50}, C_c, $\tan\phi$, L, σ_n).

Table 5. Accuracy of the surrogate models for different levels of smoothing

Smoothing (λ)	RSME (kN/m)	RSME/STD	E_1'	d_r	$\sum_u S_u$
0.01	1.04	0.05	0.93	0.97	0.877
1	2.3	0.12	0.84	0.92	0.910
100	5.7	0.33	0.58	0.79	0.991

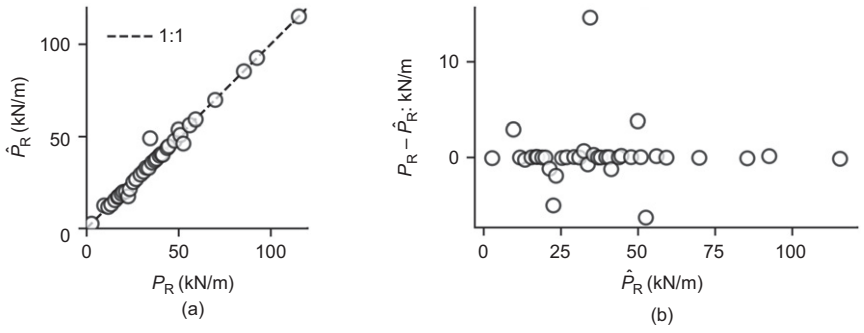

Figure 6. Accuracy of the surrogate model in predicting ultimate pullout resistance for $\lambda = 0.01$: (a) comparison of the measured (P_R) and predicted ($\hat{P}_R$) pullout resistance (b) residuals ($P_R - \hat{P}_R$) as a function of the predicted pullout resistance

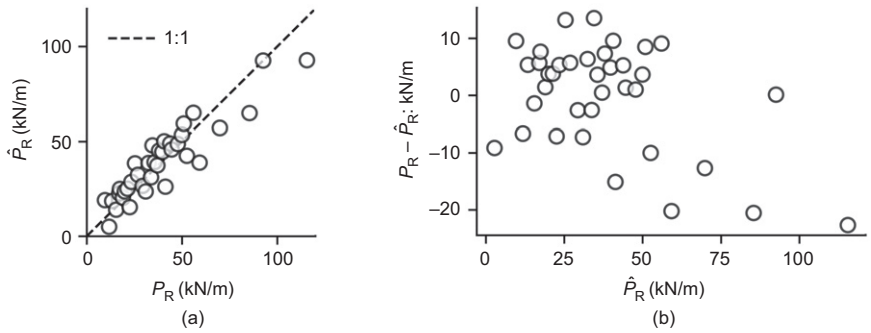

Figure 7. Accuracy of the surrogate model in predicting ultimate pullout resistance for $\lambda = 100$: (a) comparison of the measured (P_R) and predicted ($\hat{P}_R$) pullout resistance (b) residuals ($P_R - \hat{P}_R$) as a function of the predicted pullout resistance

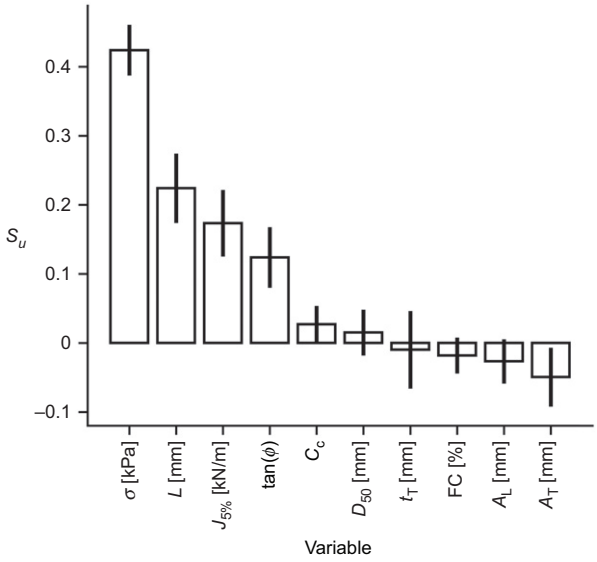

Figure 8. Sensitivity of ultimate pullout resistance to the ten most significant variables ($\lambda = 0.01$)

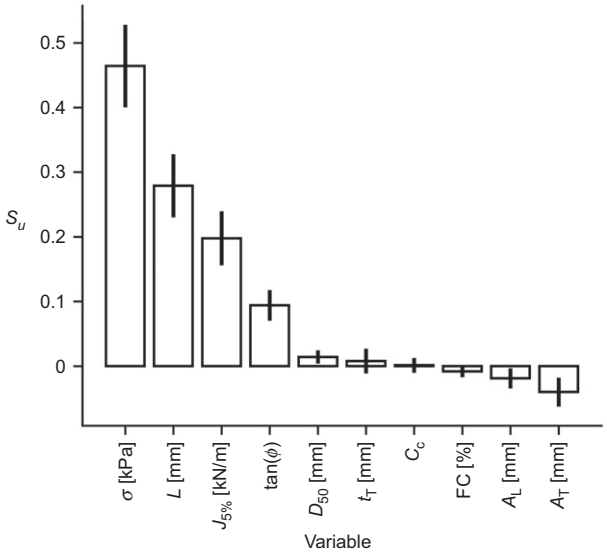

Figure 9. Sensitivity of ultimate pullout resistance to the ten most significant variables ($\lambda = 100$)

At $\lambda = 100$, the RSME/STD was still lower than the limit of 0.5 recommended by Moriasi *et al.* (2007). However, E_1' and d_r has decreased to 0.58 and 0.79, respectively. Thus, at higher degrees of smoothing the ability of the surrogate model to accurately represent the original data decreases.

Based on the *k*-fold validation results, surrogate modelling was judged to have the capacity to accurately model the relationship between pullout resistance and the input variables. Thus, surrogate models were used to smooth the dataset. The full dataset was used to fit the surrogate surface that was used to smooth the dataset. This smoothed dataset was used as input to the HDMR modelling. Due to the limited size of the dataset the HDMR analysis was restricted to a first order analysis (i.e. combinations of variables were not considered). Third order polynomials were used to approximate the target function.

The total sensitivity of pullout resistance to the ten variables is shown in Figure 8 for the dataset smoothed with $\lambda = 0.01$ (i.e. negligible smoothing). The $p = 0.05$ confidence interval for each value is also shown. For this analysis the sum of the total sensitivities was 0.88 (see Table 5). Thus, the results of the sensitivity analysis were unreliable. In contrast, the results of the sensitivity analysis applied to the dataset smoothed with $\lambda = 100$ are shown in Figure 9. For this analysis the sum of the total sensitivity approximated unity (see Table 5), and the results were reliable. Thus, as the degree of smoothing (λ) increased, the accuracy of the surrogate surface used to smooth the datapoints decreased, but the reliability of the results of the sensitivity analysis increased. Nevertheless, the variables to which P_r was the most sensitive were consistently σ, L, $J_{5\%}$ and tanϕ.

Of the four key variables, three are considered in the simplified linear model (see Equation (6)) – that is σ, L and tanϕ. These three variables were responsible for 84% in the variance in P_r in this dataset (for $\lambda = 100$). An additional 19% of variance was due to $J_{5\%}$, a variable that is not considered in the simplified models.

In both Figures 8 and 9 the sensitivity to A_L and A_T is negative. This implies that increasing the variance of these two variables decreases the variance in pullout resistance. The total sensitivity is the sum of the structural and the correlative sensitivities. For both A_L and A_T it was the correlative component that was negative. In some models the negative correlation may have a physical explanation

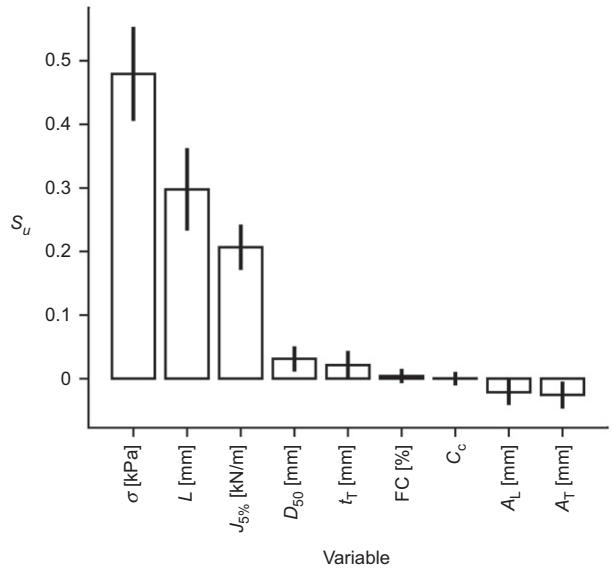

Figure 10. Sensitivity of ultimate pullout resistance to the ten most significant variables, when tanϕ is not considered as a variable ($\lambda = 100$)

(Gao *et al*. 2023), however, in this study it is assumed that the negative values are the artefact of the limited size of the dataset.

The soil grading descriptors, D_{50}, C_C and FC had a negligible effect on the P_R. There are three possible explanations for this behaviour. Firstly, the friction angle of the soil reflects the D_{50} and FC of the soil (consider the correlation in Figure 5). When tanϕ is not considered as input to the surrogate model for P_R, the sensitivity of P_R to D_{50} increased slightly as shown in Figure 10.

Secondly, the dataset consists mostly of soils with good interaction with the geogrid. Thus, the interaction between the particle size distribution and geogrid geometry fails to register in the sensitivity analysis. For most of the soil-geogrid combinations considered, t_T/D_{50} was less than 10 (see Section 2.2.1), as shown in Figure 11a.

Thirdly, the products in the dataset were fairly homogenous due to the large number of uniaxial geogrids. The distribution of A_T/D_{50} and A_L/D_{50} for the dataset is presented in Figure 11b. Both distributions are skewed towards the right, with a similar mode and median. Therefore, not much variability can be observed in terms

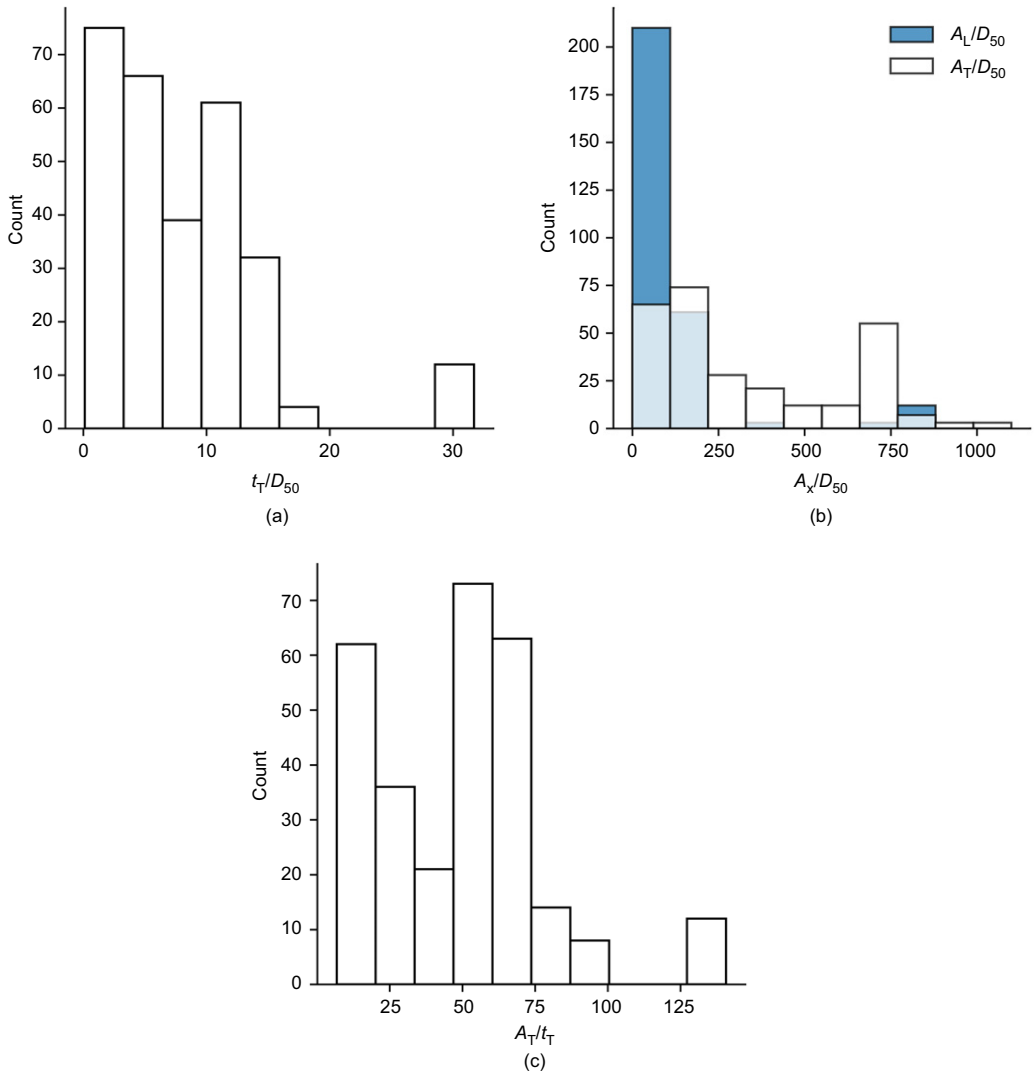

Figure 11. Distributions of the ratios indicative of soil-geogrid interaction behaviour for the dataset considered: (a) transverse rib thickness to D_{50} ratio, (b) aperture size to D_{50} ratio and (c) aperture size to transverse rib thickness ratio

of the ratio of the aperture size to D_{50}. The large A_x/D_{50} values contradict the optima of 1.25 and 3.75 reported in Section 2.2.1. This may be a result of the manufacturers' attempts to minimize interference by increasing A_T/t_T to exceed 40 (see Section 2.2.2) as shown in Figure 11c.

3.3. Regression analysis of pullout resistance

The sensitivity analysis revealed that, in addition to the variables considered in the simplified linear model, P_R was sensitive to $J_{5\%}$. In this section, the effect of including additional variables in the regression models is evaluated.

3.3.1. *Regression analysis on the variables of the simplified linear model*

Multiple linear regression was done using the *Statsmodels* Python package (Seabold and Perktold 2010). Following the simplified linear model (Equation (6)) and the non-linear model by Huang and Bathurst (2009), the models for P_R were assumed to follow the form:

$$P_R = 2\beta_0 \prod_i X_i^{\beta_i} \tag{16}$$

That is, the product of the variables (X_i), each raised to a constant (β_i), multiplied with a constant (β_0). To set up the models for linear regression, the following log transform was used:

$$\log P_R = \log 2\beta_0 + \sum_i (\beta_i \log X_i + \varepsilon_i) \tag{17}$$

where ε_i is the random error at each point assumed to be normally distributed (Kutner 2005).

For a robust comparison of the different regression models, k-fold cross validation was implemented (Kutner 2005). The dataset was randomly split into five 'folds' of equal size using the stratified sampling technique discussed in Section 3.2.1. Each fold was then used to calculate the performance of a model trained on the remaining four folds. Finally, the average of the performance metrics (RMSE, E_1', d_r) for the five iterations was calculated.

The first model analysed was used as a baseline. The model followed the form of the simplified linear model (Equation (6)), – that is, $P_r = 2\beta_0 L\sigma\tan\phi$. The ratio of the average RMSE in log space ($RMSE_{log,avg}$) to the standard deviation of the complete dataset in log space (STD_{log}) was 0.76 (see Table 6). The average E_1' and d_r were 0.21 and 0.61, respectively.

For illustrative purposes the model was also fitted to the full dataset. Figure 12a presents the predicted $\log \hat{P}_R$ as a function of the measured $\log P_R$ for the baseline model fitted to the full dataset. The equivalent results in linear space are shown in Figure 12c. The poor fit of the model to the data is reflected in the distribution of residuals depicted in Figure 12b. A clear downward trend in the residuals is apparent with an increase in $\log \widehat{P}_r$.

The second model considered the parameters of the simplified linear model, but assumed the relationship with P_R to be non-linear: $P_R = 2\beta_0 L^{\beta_1}\sigma^{\beta_2}(\tan\phi)^{\beta_3}$. The $RMSE_{log,avg}/STD_{log}$ for the non-linear baseline model was 0.51, which was an improvement over the linear model. In Figure 13a, the ultimate pullout resistance predicted by the non-linear baseline model, fitted to the full dataset, is compared to the measured pullout resistance. Figure 13c shows the equivalent relationship on a linear scale. The residuals in Figure 13b had less structure than the ones for the linear, baseline model in Figure 12b. Thus, non-linearity has been sufficiently accounted for by this updated model.

Table 6. Summary of model performance in log space, based on average from k-fold validation

Model name	Model form	$RMSE_{log,avg}/STD_{log}$	E_1'	d_r
Baseline	$2\beta_0 L\sigma\tan\phi$	0.76	0.21	0.61
Baseline, non-linear	$2\beta_0 L^{\beta_1}\sigma^{\beta_2}(\tan\phi)^{\beta_3}$	0.51	0.51	0.75
Expanded	$\beta_0 L^{\beta_1}\sigma^{\beta_2}(\tan\phi)^{\beta_3} J_{5\%}^{\beta_4} A_T^{\beta_5} FC^{\beta_6}$	0.43	0.58	0.79
Alternative 1	$2\beta_0(\sigma_n\tan\phi J_{5\%}L)^{0.5}$	0.52	0.50	0.75
Alternative 2	$2\beta_0(\sigma_n\tan\phi J_{5\%}L)^{0.5}\left(\frac{D_{50}}{A_T}\right)^{\beta_1} FC^{\beta_1}$	0.46	0.54	0.77

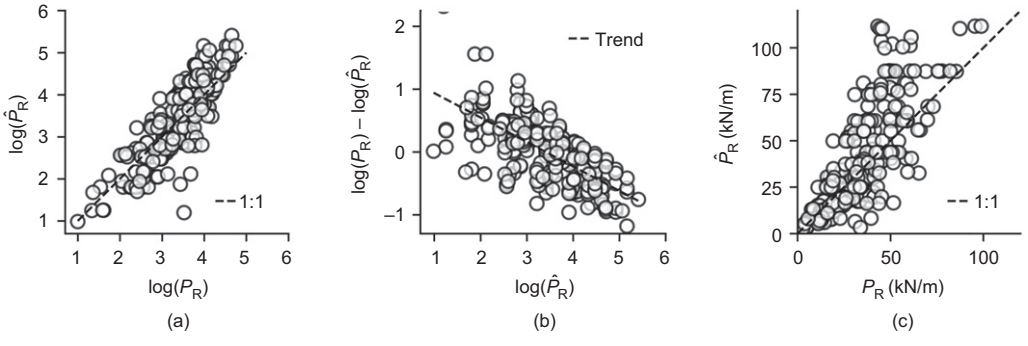

Figure 12. Baseline model ($P_r = 2.k.L.\sigma.\tan\phi$) fitted to the full dataset: (a) and (c) predicted versus measured ultimate pullout resistance, (b) residuals of the model

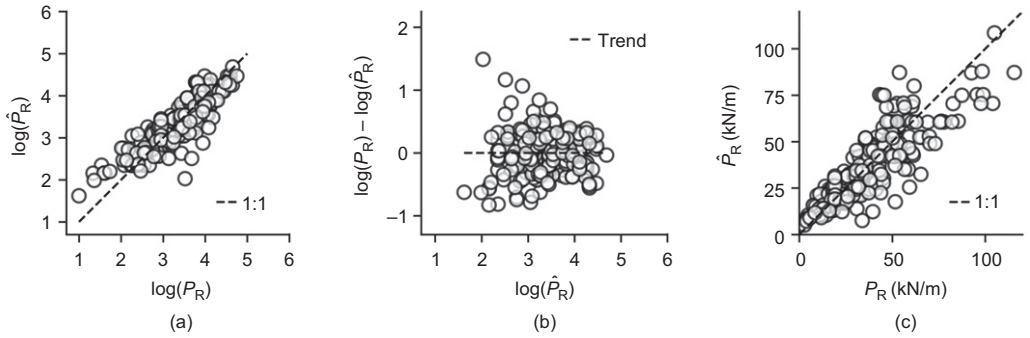

Figure 13. Non-linear model ($P_R = 2.\beta_0.L^{\beta_1}.\sigma^{\beta_2}.(\tan\phi)^{\beta_3}$) fitted to the complete dataset: (a) and (c) predicted versus measured ultimate pullout resistance, (b) residuals of the model

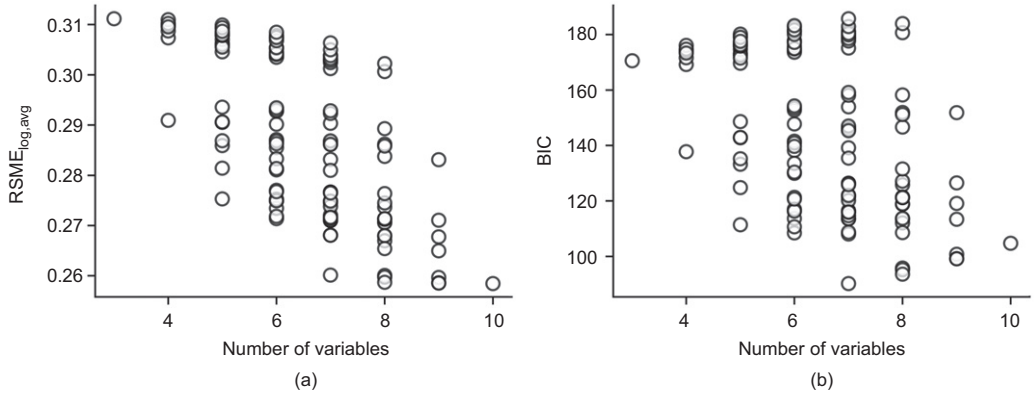

Figure 14. Quality of regression models as a function of the number of variables: (a) RSME$_{log,avg}$ and (b) BIC

The model coefficients for the complete dataset were:

$$P_r = (2)(7.7)L^{0.86}\sigma_n^{0.52}(\tan\phi)^{0.89} \quad (18)$$

where L has units of meters and σ_n units of kPa. While the non-linear relationship with σ_n and L is often identified in the literature, little mention is made of the non-linear relationship between P_R and tanϕ.

3.3.2. *Regression analysis considering the additional variables*

The two models analysed in Section 3.3.1 only considered the variables of the simplified linear model. Based on the sensitivity analysis in Section 3.2.3 additional variables may be required to accurately model P_R. To determine the ideal number of variables, a model was created for all combinations of the additional variables (A_T, A_L, t_T, $J_{5\%}$, FC, D_{50}, C_c) together with σ_n, L and tanϕ. The family of models was compared based on the RMSE$_{log,avg}$ and Bayesian Information Criterion (BIC) (Schwarz 1978). The BIC is a metric that balances the accuracy of the model against the number of parameters, – that is, it is used to identify overfitting. A lower BIC value is preferred.

The RMSE$_{log,avg}$ and the BIC for the models are shown in Figure 14 as a function of the number of variables. The BIC was calculated for models fitted to the full dataset. The RSME$_{log,avg}$ represented the average of the k-fold validation. For more than seven variables the reduction in RMSE with the addition of a new variable plateaued, which corresponds to the minimum BIC value.

The expanded model with seven variables, corresponding to the minimum BIC had the form:

$$P_R = 2.011{\cdot}L^{0.80}\sigma_n^{0.52}(\tan\phi)^{0.53}J_{5\%}^{0.33}A_T^{-0.12}D_{50}^{0.13}\mathrm{FC}^{0.035} \quad (19)$$

where L, A_T and A_L have units of meters, σ_n has units of kPa and $J_{5\%}$ has units in kN/m. The RMSE$_{log,avg}$/STD$_{log}$ for the model was 0.43, representing a 44% improvement on the baseline model and a 15% improvement on the baseline non-linear model.

The coefficients for L and σ_n were similar to those of the nonlinear model in Equation (18). In addition, $J_{5\%}$, A_T, D_{50} and FC formed part of the model with the lowest BIC. An increase in $J_{5\%}$, D_{50} and FC was associated with an increase in P_R. The P_R increased as the spacing of the transverse ribs (A_T) decreased, – that is, as the number of transverse ribs increased. However, corresponding to the results of the sensitivity analysis, the regression coefficients of A_T, D_{50} and FC were small, suggesting that the variables are of limited significance.

3.3.3. *Alternatives to the simplified linear model*

The non-linear model in Equation (18) and the expanded model in Equation (19) showed a clear improvement in prediction accuracy on the baseline model. However, both models are not dimensionally consistent. Two alternatives to the baseline model are proposed. These models expand

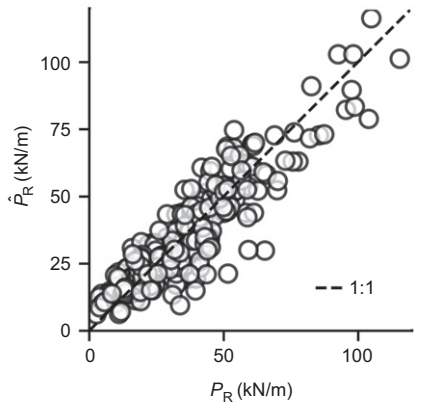

Figure 15. Predicted versus measured ultimate pullout resistance for the first alternative model

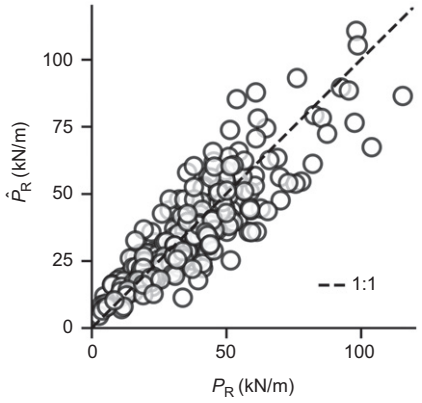

Figure 16. Predicted versus measured ultimate pullout resistance for the second alternative model

on the variables of the baseline model, are non-linear, and are dimensionally consistent.

The first alternative model considers $J_{5\%}$ in addition to variables of the baseline model:

$$P_R = 2\beta_0(\sigma_n \tan\phi J_{5\%} L)^{0.5} \quad (20)$$

The coefficient β_0 was 0.48 for the model fitted to the full dataset. A plot of $\hat{P}_R$ versus P_R for the first alternative model is shown in Figure 15. The $RMSE_{log,avg}/STD_{log}$ of 0.50 was comparable to the non-linear baseline model, while maintaining consistency amongst the dimensions. This model was a 34% improvement on the baseline model.

For the second alternative model $J_5\%$, TR_A, D_{50} and FC was considered in addition to σ, L and $\tan\phi$:

$$P_R = 2\beta_0(\sigma_n \tan\phi J_{5\%} L)^{0.5}\left(\frac{D_{50}}{TR_A}\right)^{\beta_1} FC^{\beta_2} \quad (21)$$

The coefficients β_0, β_1 and β_2 were 0.348, 0.14 and 0.04 respectively when the model was fitted to the full dataset. A comparison of the predicted and measured pullout resistance is shown in Figure 16. The performance of this model was comparable to the expanded model in Equation (19), while being dimensionally consistent (see Table 6). However, this increase in performance was not sufficient to justify the increased complexity of the second alternative model.

It should be noted that these alternative models are purely empirical. Unlike the simplified linear models, the form of the alternative models is not grounded in the physics of the problem. Furthermore, the dataset analysed in this study was too limited to recommend a general alternative model to the FHWA and EBGEO models. The dataset contains a non-negligible fraction of unconventional backfills and is dominated by a single family of geogrids (HDPE, unitized, uniaxial). However, the increased accuracy of the non-linear alternative models suggests that subsequent design model updates should as a minimum consider the non-linearity of ultimate pullout resistance as well as the contribution of geogrid stiffness.

4. CONCLUSIONS

This work presented a review of geogrid ultimate pullout capacity modelling. An investigation of analytical models for predicting ultimate pullout resistance found that the geogrid structure is often considered in modelling but not the mechanical response. Furthermore, limited consideration is given to the effect of soil particle size and particle size distribution on soil-geogrid interaction. The remainder of the work focused on the effect of geogrid geometry and soil particle size distribution.

A sensitivity analysis was conducted to evaluate the significance of the geogrid mechanical response and soil particle size distribution on the ultimate pullout resistance. The sensitivity analysis indicated that ultimate pullout resistance in this dataset was most sensitive to normal stress (σ_n), followed by length (L), the stiffness of the geogrid ($J_{5\%}$), and friction angle (ϕ). Normal stress (σ_n), length (L), and friction angle (ϕ) form the backbone of the simplified linear models (FHWA and EBGEO). The particle size distribution of the soils considered in this dataset was found not to have a significant impact on the ultimate pullout resistance.

Finally, the significance of the modelling pullout resistance with additional variables was evaluated using a regression model. The baseline model considered only L, σ_n and ϕ. Based on the RMSE and Bayes Information Criterion, increasing the number of regression variables above seven resulted in negligible gains in model accuracy. When considering the seven most significant variables, L, σ_n, ϕ, $J_{5\%}$, D_{50}, A_T and FC, the prediction of ultimate pullout resistance improved with 44% on the baseline linear model and 15% on a baseline model incorporating non-linearity. An alternative to the baseline model was then proposed that considers $J_{5\%}$ in addition to L, σ_n and ϕ, maintains dimensional consistency and considers the non-linear response of the ultimate pullout resistance. The alternative model showed a 32% improvement on the baseline linear model.

ACKNOWLEDGEMENTS

The authors are grateful to Tensar International Corporation for the financial assistance provided for the study. Opinions expressed and conclusions presented

are solely those of the authors. The first author is also thankful for the support provided by a Harrington Dissertation Fellowship.

NOTATION

Basic SI units are shown in parentheses.

A, A_L, A_T	geogrid aperture size (mm)
A_b	bearing area of the transverse ribs (mm^2)
C_u	coefficient of uniformity: D_{60}/D_{10} (dimensionless)
C_z	coefficient of curvature: $D_{30}^2/(D_{60}D_{10})$ (dimensionless)
c	intercept of the Mohr Coulomb failure surface (kPa)
D_{XX}	particle size greater than XX% of the particles (mm)
d_r	index of agreement (dimensionless)
E_1'	adjusted coefficient of efficiency (dimensionless)
F^*	pullout resistance factor (dimensionless)
FC	fines content of the soil (dimensionless)
f_b	bearing resistance factor (dimensionless)
$f_{sg,k}$	friction coefficient (dimensionless)
f_u	component function (dimensionless)
$J_{x\%}$	secant tensile modulus at x% tensile strain (kN/m)
L	anchorage length (m)
L_A	active length of the geogrid (m)
P_R	ultimate pullout resistance (measured) (kN)
$\hat{P}_R$	ultimate pullout resistance (predicted) (kN)
$P_{R,B}$	bearing component of P_R (kN)
$P_{R,F}$	frictional component of P_R (kN)
R	Pearson's correlation coefficient (dimensionless)
RMSE	root mean squared error (dimensionless)
$RMSE_{log,avg}$	average of the RMSE in log space (dimensionless)
S_i	first order effect (dimensionless)
S_L	longitudinal rib spacing (mm)
S_T	transverse rib spacing (mm)
S_u	total sensitivity (dimensionless)
S_u^b	structural sensitivity (dimensionless)
S_u^b	correlative sensitivity (dimensionless)
T	unit tension (kN/m)
T_{Ult}	ultimate tensile strength (kN/m)
t_{avg}	average transverse rib thickness (mm)
t_t	transverse rib thickness (mm)
w	shear band width (mm)
w_j	weight of basis function i (dimensionless)
X_i	distribution of variable X (dimensionless)
$1+\kappa$	non-linear correction factor for P_R (dimensionless)
α	scale correction factor (dimensionless)
α_f	fraction of the geogrid area that is solid (dimensionless)
β	non-linear correction factor for P_R (dimensionless)
β_x	regression coefficient (dimensionless)
δ	soil-geogrid interface friction angle (°)
ε	random error (dimensionless)
λ	smoothing parameter for the surrogate surface (dimensionless)
μ_{AL}	apparent coefficient of soil-geogrid interface friction (dimensionless)
ρ	Spearman's correlation coefficient (dimensionless)
σ	standard deviation (dimensionless)
σ_b	bearing resistance (kPa)
σ_n	normal stress (kPa)
τ	soil-geogrid interface shear stress (kPa)
ϕ	soil friction angle (°)
$\phi_j(x, x_c^j)$	basis function centred about x_c^j (dimensionless)

ABBREVIATIONS

BIC	Bayesian Information Criterion
DEM	Discrete Element Modelling
EBGEO	'*Empfehlungen für den Entwurf und die Berechnung von Erdkörpern mit Bewehrungen aus Geokunststoffen*' (Recommendations for Design and Analysis of Earth Structures using Geosynthetic Reinforcements)
FHWA	Federal Highway Administration
HDMR	High Dimensional Model Representation
HDPE	High Density Polyethene
MDD	Maximum Dry Density
PET	Polyethylene Terephthalate
PP	Polypropylene
RMSE	Root Mean Squared Error
STD	Standard Deviation

REFERENCES

Abdi, M. R. & Mirzaeifar, H. (2017). Experimental and PIV evaluation of grain size and distribution on soil–geogrid interactions in pullout test. *Soils and Foundations*, **57**, No. 6, 1045–1058, https://doi.org/10.1016/j.sandf.2017.08.030.

Abramento, M. & Whittle, A. J. (1993). Shear-lag analysis of planar soil reinforcement in plane-strain compression. *Journal of Engineering Mechanics*, **119**, No. 2, 270–291, https://doi.org/10.1061/(ASCE)0733-9399(1993)119:2(270).

Abu-Farsakh, M. Y., Almohd, I. & Farrag, K. (2006). Comparison of field and laboratory pullout tests on geosynthetics in marginal soils. *Transportation Research Record*, **1975**, 124–136, https://doi.org/10.1177/0361198106197500114.

Alfaro, M., Miura, N. & Bergado, D. (1995a). Soil-geogrid reinforcement interaction by pullout and direct shear tests. *Geotechnical Testing Journal*, **18**, No. 2, 157, https://doi.org/10.1520/GTJ10319J.

Alfaro, M. C., Hayashi, S., Miura, N. & Watanabe, K. (1995b). Pullout interaction mechanism of geogrid strip reinforcement. *Geosynthetics International*, **2**, No. 4, 679–698, https://doi.org/10.1680/gein.2.0030.

Alobaidi, I. A., Hoare, D. J. & Ghataora, G. S. (1997). Load transfer mechanism in pull-out tests. *Geosynthetics International*, **4**, No. 5, 509–521, https://doi.org/10.1680/gein.4.0104.

Alshibli, K. A. & Sture, S. (1999). Sand shear band thickness measurements by digital imaging techniques. *Journal of Computing in Civil Engineering*, **13**, No. 2, 103–109, https://doi.org/10.1061/(ASCE)0887-3801(1999)13:2(103).

Anderson, N. H. & Shanteau, J. (1977). Weak inference with linear models. *Psychological Bulletin*, **84**, No. 6, 1155–1170, https://doi.org/10.1037/0033-2909.84.6.1155.

Ang, A. H. S. & Tang, W. H. (2007). *Probability Concepts in Engineering: Emphasis on Applications in Civil & Environmental Engineering*, 2nd edn, Wiley, New York, NJ, USA.

ASTM D6706-01 *Test Method for Measuring Geosynthetic Pullout Resistance in Soil*. ASTM International, West Conshohocken, PA, USA.

Berg, R. R., Christoper, B. R. & Samtani, N. C. (2009). *Design and Construction of Mechanically Stabilized Earth Walls and Reinforced Soil Slopes – Volume I*, Federal Highway Administration, Washington, DC, USA, p. 306.

Bergado, D. T. & Chai, J. C. (1994). Pullout force/displacement relationship of extensible grid reinforcements. *Geotextiles and Geomembranes*, **13**, No. 5, 295–316, https://doi.org/10.1016/0266-1144(94)90025-6.

Bergado, D. T., Bukkanasuta, A. & Balasubramaniam, A. S. (1987). Laboratory pull-out tests using bamboo and polymer geogrids including a case study. *Geotextiles and Geomembranes*, **5**, No. 3, 153–189, https://doi.org/10.1016/0266-1144(87)90015-X.

Birnbaum, M. H. (1973). The devil rides again: correlation as an index of fit. *Psychological Bulletin*, **79**, No. 4, 239–242, https://doi.org/10.1037/h0033853.

Brown, S. F., Kwan, J. & Thom, N. H. (2007). Identifying the key parameters that influence geogrid reinforcement of railway ballast. *Geotextiles and Geomembranes*, **25**, No. 6, 326–335, https://doi.org/10.1016/j.geotexmem.2007.06.003.

Calvarano, L. S. (2012). *Behavior of Different Geogrids under Static and Cyclic Pullout Conditions (In Italian: Comportamento di Differenti Geogriglie in Condizione di Sfilamento Statico e Ciclico)*, PhD dissertation, Mediterranean University of Reggio Calabria, Reggio Calabria, Italy.

Calvarano, L. S., Cardile, G., Moraci, N. & Recalcati, P. G. (2012). The influence of reinforcement geometry and soil types on the interface behaviour in pullout conditions. In *Proceedings of the 5th European Conference on Geosynthetics*, Blanco, M., Leiro, A., Mateio, B., Torregrosa, J. B., Abad, F., Pardo de Santayana, F. & Santalla, J., Editors, Valencia, Spain, p. 7.

Cardile, G., Moraci, N. & Calvarano, L. S. (2016). Geogrid pullout behaviour according to the experimental evaluation of the active length. *Geosynthetics International*, **23**, No. 3, 194–205, https://doi.org/10.1680/jgein.15.00042.

Cardile, G., Gioffrè, D., Moraci, N. & Calvarano, L. S. (2017). Modelling interference between the geogrid bearing members under pullout loading conditions. *Geotextiles and Geomembranes*, **45**, No. 3, 169–177, https://doi.org/10.1016/j.geotexmem.2017.01.008.

Castelvecchi, D. (2016). Can we open the black box of AI? *Nature News*, **538**, No. 20–30, https://doi.org/10.1038/538020a.

Christopher, B. R., Gill, S. A., Giroud, J. P., Juran, I., Mitchell, J. K., Schlosser, F. & Dunnicliff, J. (1989). *Reinforced Soil Structures Volume II: Summary Of Research and Systems Information*, Federal Highway Administration, McLean, VA, USA.

Christopher, B. R., Gill, S., Giroud, J. P., Juran, I., Mitchell, J. K., Schlosser, F. & Dunnicliff, J. (1990). *Reinforced Soil Structures Volume I: Design and Construction Guidelines*, U.S. Department of Transportation Publication, McLean, VA, USA.

Collin, J. G., Stark, T. D., Lucarelli, A., Taylor, T. P. & Berg, R. R. (2021). Stability and stress-deformation analyses of reinforced slope failure at Yeager airport. *Journal of Geotechnical and Geoenvironmental Engineering*, **147**, No. 3, 04020179, https://doi.org/10.1061/(ASCE)GT.1943-5606.0002454.

Derksen, J., Fuentes, R. & Ziegler, M. (2022). Geogrid-soil interaction: experimental analysis of factors influencing load transfer. *Geosynthetics International*, **30**, No. 3, 1–22, https://doi.org/10.1680/jgein.21.00110.

Desrues, J. & Viggiani, G. (2004). Strain localization in sand: an overview of the experimental results obtained in Grenoble using stereophotogrammetry. *International Journal for Numerical and Analytical Methods in Geomechanics*, **28**, No. 4, 279–321, https://doi.org/10.1002/nag.338.

Dyer, M. R. (1985). *Observations of the Stress Distribution in Crushed Glass with Applications to Soil Reinforcement*, PhD dissertation, University of Oxford, Oxford, UK.

Farrag, K., Acar, Y. B. & Juran, I. (1993). Pull-out resistance of geogrid reinforcements. *Geotextiles and Geomembranes*, **12**, No. 2, 133–159, https://doi.org/10.1016/0266-1144(93)90003-7.

Gao, Y., Sahin, A. & Vrugt, J. A. (2023). Probabilistic sensitivity analysis with dependent variables: covariance-based decomposition of hydrologic models. *Water Resources Research*, **59**, No. 4, e2022WR032834, https://doi.org/10.1029/2022WR032834.

German Geotechnical Society (2011). *Recommendations for Design and Analysis of Earth Structures using Geosynthetic Reinforcements – EBGEO*, 2nd edn, Johnson, A., Editor, Wilhelm Ernst & Sohn, Berlin, Germany. See https://onlinelibrary.wiley.com/doi/book/10.1002/9783433600931 (accessed 27/09/2023).

Goodhue, M. J., Edil, T. B. & Benson, C. H. (1998). *Reuse of Foundry Sands in Reinforced Earthen Structures*, University of Wisconsin-Madison, Madison, WI, USA, Environmental Geotechnic Report 98-16.

Guo, P. (2012). Critical length of force chains and shear band thickness in dense granular materials. *Acta Geotechnica*, **7**, No. 1, 41–55, https://doi.org/10.1007/s11440-011-0154-3.

Gurung, N. & Iwao, Y. (1999). Comparative model study of geosynthetic pull-out response. *Geosynthetics International*, **6**, No. 1, 53–68, https://doi.org/10.1680/gein.6.0143.

Han, B., Ling, J., Shu, X., Gong, H. & Huang, B. (2018). Laboratory investigation of particle size effects on the shear behavior of aggregate-geogrid interface. *Construction and Building Materials*, **158**, No. 15, 1015–1025, https://doi.org/10.1016/j.conbuildmat.2017.10.045.

Herman, J. & Usher, W. (2017). SALib: an open-source python library for sensitivity analysis. *The Journal of Open Source Software*, **2**, No. 9, 97, https://doi.org/10.21105/joss.00097.

Huang, B. & Bathurst, R. J. (2009). Evaluation of soil-geogrid pullout models using a statistical approach. *Geotechnical Testing Journal*, **32**, No. 6, 489–504, https://doi.org/10.1520/GTJ102460.

Indraratna, B., Karimullah Hussaini, S. K. & Vinod, J. S. (2012). On the shear behavior of ballast-geosynthetic interfaces. *Geotechnical Testing Journal*, **35**, No. 2, 103317, https://doi.org/10.1520/GTJ103317.

Indraratna, B., Hussaini, S. K. K. & Vinod, J. S. (2013). The lateral displacement response of geogrid-reinforced ballast under cyclic loading. *Geotextiles and Geomembranes*, **39**, 20–29, https://doi.org/10.1016/j.geotexmem.2013.07.007.

Jacobs, F., Ziegler, M., Vollmert, L. & Ehrenberg, H. (2014). Explicit design of geogrids with a nonlinear interface model. In *Proceedings of the 10th International Conference on Geosynthetics*, Deutsche Gesellschaft Fuer Geotechnik, Berlin, Germany, pp. 609–616.

Jewell, R. A. (1990). Reinforcement bond capacity. *Géotechnique*, **40**, No. 3, 6.

Jewell, R. A., Milligan, G. W. E., Sarsby, R. W. & Dubois, D. (1985). Interaction between soil and geogrids. In *Polymer Grid Reinforcement*, Thomas Telford Publishing, London, UK, pp. 18–30.

Kang, M., Kim, J. H., Qamhia, I. I. A., Tutumluer, E. & Wayne, M. H. (2020). Geogrid stabilization of unbound aggregates evaluated through bender element shear wave measurement in repeated load triaxial testing. *Transportation Research Record*, **2674**, 113–125, https://doi.org/10.1177/0361198120908230.

Koerner, R. M. (2012). *Designing with Geosynthetics*, Vol 1, 6th edn, Xlibris Corporation, Bloomington, IN, USA.

Koerner, R. M., Wayne, M. H. & Carroll, R. G. (1989). Analytic behaviour of geogrid anchorage. In *Proceedings of Geosynthetics '89*, IFAI, San Diego, CA, USA, pp. 525–636.

Kohavi, R. (1995). A study of cross-validation and bootstrap for accuracy estimation and model selection. In *Proceedings of the 14th International Joint Conference on Artificial Intelligence–Volume 2*, Mellish, C., Editor, Morgan Kaufmann Publishers Inc, Montreal, QC, Canada, pp. 1137–1143.

Kutner, M. H., Editor (2005). *Applied Linear Statistical Models*, 5th edn, McGraw-Hill Irwin, Boston, New York, NY, USA.

Legates, D. R. & McCabe, G. J. (1999). Evaluating the use of 'goodness-of-fit' measures in hydrologic and hydroclimatic model validation. *Water Resources Research*, **35**, No. 1, 233–241, https://doi.org/10.1029/1998WR900018.

Legates, D. R. & McCabe, G. J. (2013). A refined index of model performance: a rejoinder. *International Journal of Climatology*, **33**, No. 4, 1053–1056, https://doi.org/10.1002/joc.3487.

Li, G. & Rabitz, H. (2012). General formulation of HDMR component functions with independent and correlated variables. *Journal of Mathematical Chemistry*, **50**, No. 1, 99–130, https://doi.org/10.1007/s10910-011-9898-0.

Li, G., Rabitz, H., Yelvington, P. E., Oluwole, O. O., Bacon, F., Kolb, C. E. & Schoendorf, J. (2010). Global sensitivity analysis for systems with independent and/or correlated inputs. *The Journal of Physical Chemistry A*, **114**, No. 19, 6022–6032, https://doi.org/10.1021/jp9096919.

Liu, C. N., Yang, K. H. & Nguyen, M. D. (2014). Behavior of geogrid–reinforced sand and effect of reinforcement anchorage in large-scale plane strain compression. *Geotextiles and Geomembranes*, **42**, No. 5, 479–493, https://doi.org/10.1016/j.geotexmem.2014.07.007.

Liu, C., Indraratna, B. & Rujikiatkamjorn, C. (2021). An analytical model for particle-geogrid aperture interaction. *Geotextiles and Geomembranes*, **49**, No. 1, 41–44, https://doi.org/10.1016/j.geotexmem.2020.09.003.

Lo, S. R. (2003). The influence of constrained dilatancy on pullout resistance of strap reinforcement. *Geosynthetics International*, **10**, No. 2, 47–55, https://doi.org/10.1680/gein.2003.10.2.47.

Lopes, M. L. & Ladeira, M. (1996). Influence of the confinement, soil density and displacement rate on soil-geogrid interaction. *Geotextiles and Geomembranes*, **14**, No. 10, 543–554, https://doi.org/10.1016/S0266-1144(97)83184-6.

Lopes, M. J. & Lopes, M. L. (1999). Soil-geosynthetic interaction - influence of soil particle size and geosynthetic structure. *Geosynthetics International*, **6**, No. 4, 261–282, https://doi.org/10.1680/gein.6.0153.

Madhav, M. R., Gurung, N. & Iwao, Y. (1998). A theoretical model for the pull-out response of geosynthetic reinforcement. *Geosynthetics International*, **5**, No. 4, 399–424, https://doi.org/10.1680/gein.5.0128.

Matsui, T., San, K. C., Nabeshima, Y. & Amin, U. N. (1996). Bearing mechanism of steel reinforcement in pull-out test. In *Earth Reinforcement*, Ochiai, H., Yasufuku, N. & Omine, K., Editors, Balkema, Fukuoka, Japan, pp. 101–105.

McDowell, G. R., Harireche, O., Konietzky, H., Brown, S. F. & Thom, N. H. (2006). Discrete element modelling of geogrid-reinforced aggregates. *Proceedings of the Institution of Civil Engineers - Geotechnical Engineering*, **159**, No. 1, 35–48, https://doi.org/10.1680/geng.2006.159.1.35.

Miao, C., Jia, Y., Zhang, J. & Zhao, J. (2020). DEM simulation of the pullout behavior of geogrid-stabilized ballast with the optimization of the coordination between aperture size and particle diameter. *Construction and Building Materials*, **255**, 119359, https://doi.org/10.1016/j.conbuildmat.2020.119359.

Milligan, G. W. E., Earl, R. F. & Bush, D. I. (1990). Observations of photoelastic pullout tests on geotextiles and geogrids. In *4th International Conference on Geotextiles, Geomembranes and Related Products*, Hoedt, G. D., Editor, Balkema, The Hague, the Netherlands, vol. 2, pp. 747–751.

Miyata, Y. & Bathurst, R. J. (2012). Reliability analysis of soil-geogrid pullout models in Japan. *Soils and Foundations*, **52**, No. 4, 620–633, https://doi.org/10.1016/j.sandf.2012.07.004.

Moraci, N. & Recalcati, P. (2006). Factors affecting the pullout behaviour of extruded geogrids embedded in a compacted granular soil. *Geotextiles and Geomembranes*, **24**, No. 4, 220–242, https://doi.org/10.1016/j.geotexmem.2006.03.001.

Moraci, N., Gioffre', D., Romano, G., Montanelli, F. & Rimoldi, P. (2002). Pullout behaviour of geogrid embedded in granular soils. In *Proceedings of the 7th International Conference on Geosynthetics*, Nice, France, Delmas, P., Gourc, J. P. & Girard, H., Editors, Swets & Zeitlinger, Lisse, Netherlands, p. 5.

Moriasi, D. N., Arnold, J. G., Van Liew, M. W., Bingner, R. L., Harmel, R. D. & Veith, T. L. (2007). Model evaluation guidelines for systematic quantification of accuracy in watershed simulations. *Transactions of the ASABE*, **50**, No. 3, 885–900, https://doi.org/10.13031/2013.23153.

Mühlhaus, H. B. & Vardoulakis, I. (1987). The thickness of shear bands in granular materials. *Géotechnique*, **37**, No. 3, 271–283, https://doi.org/10.1680/geot.1987.37.3.271.

Ochiai, H., Otani, J., Hayashic, S. & Hirai, T. (1996). The pull-out resistance of geogrids in reinforced soil. *Geotextiles and Geomembranes*, **14**, No. 1, 19–42, https://doi.org/10.1016/0266-1144(96)00027-1.

Oda, M. & Kazama, H. (1998). Microstructure of shear bands and its relation to the mechanisms of dilatancy and failure of dense granular soils. *Géotechnique*, **48**, No. 4, 465–481, https://doi.org/10.1680/geot.1998.48.4.465.

Ovesen, N. K. (1979). The scaling law relationship - panel discussion. In *Proceedings of the 7th European Conference on Soil Mechanics and Foundations*, Brighton, UK, pp. 319–323.

Palmeira, E. M. (2004). Bearing force mobilisation in pull-out tests on geogrids. *Geotextiles and Geomembranes*, **22**, No. 6, 481–509, https://doi.org/10.1016/j.geotexmem.2004.03.007.

Palmeira, E. M. (2009). Soil–geosynthetic interaction: modelling and analysis. *Geotextiles and Geomembranes*, **27**, No. 5, 368–390, https://doi.org/10.1016/j.geotexmem.2009.03.003.

Palmeira, E. M. & Milligan, G. W. E. (1989). Scale and other factors affecting the results of pull-out tests of grids buried in sand. *Géotechnique*, **39**, No. 3, 511–524, https://doi.org/10.1680/geot.1989.39.3.511.

Pant, A. & Ramana, G. V. (2022). Prediction of pullout interaction coefficient of geogrids by extreme gradient boosting model. *Geotextiles and Geomembranes*, **50**, No. 6, 1188–1198, https://doi.org/10.1016/j.geotexmem.2022.08.003.

Pant, A., Datta, M. & Ramana, G. V. (2019a). Bottom ash as a backfill material in reinforced soil structures. *Geotextiles and Geomembranes*, **47**, No. 4, 514–521, https://doi.org/10.1016/j.geotexmem.2019.01.018.

Pant, A., Datta, M., Ramana, G. V. & Bansal, D. (2019b). Measurement of role of transverse and longitudinal members on pullout resistance of PET geogrid. *Measurement*, **148**, 106944, https://doi.org/10.1016/j.measurement.2019.106944.

Pant, A., Ramana, G. V., Datta, M. & Gupta, S. K. (2019c). Coal combustion residue as structural fill material for reinforced soil structures. *Journal of Cleaner Production*, **232**, 417–426, https://doi.org/10.1016/j.jclepro.2019.05.354.

Perkins, S. W. & Cuelho, E. V. (1999). Soil-geosynthetic interface strength and stiffness relationships from pullout tests. *Geosynthetics International*, **6**, No. 5, 321–346, https://doi.org/10.1680/gein.6.0156.

Prandtl, L. (1920). Regarding the rigidity of plastic bodies (in German: Über die Härte plastischer Körper). *Nachrichten von der Königlichen Gesellschaft der Wissenschaften zu Göttingen: Mathematisch-physikalische Klasse aus dem Jahre*, Weidmannsche Buchhandlung, Berlin, Germany, pp. 74–85.

Prasad, P. S. & Ramana, G. V. (2016a). Feasibility study of copper slag as a structural fill in reinforced soil structures. *Geotextiles and Geomembranes*, **44**, No. 4, 623–640, https://doi.org/10.1016/j.geotexmem.2016.03.007.

Prasad, P. S. & Ramana, G. V. (2016b). Imperial smelting furnace (zinc) slag as a structural fill in reinforced soil structures. *Geotextiles and Geomembranes*, **44**, No. 3, 406–428, https://doi.org/10.1016/j.geotexmem.2016.01.009.

Raju, D. M. & Fannin, R. J. (1998). Load-strain-displacement response of geosynthetics in monotonic and cyclic pullout. *Canadian Geotechnical Journal*, **35**, No. 2, 183–193.

Rattez, H., Shi, Y., Sac-Morane, A., Klaeyle, T., Mielniczuk, B. & Veveakis, M. (2022). Effect of grain size distribution on the shear band thickness evolution in sand. *Géotechnique*, **72**, No. 4, 350–363, https://doi.org/10.1680/jgeot.20.P.120.

Roodi, G. H. (2016). *Analytical, Experimental, and Field Evaluations of Soil-Geosynthetic Interaction under Small Displacements*, PhD dissertation, The University of Texas at Austin, Austin, TX, USA.

Saltelli, A., Ratto, M., Andres, T., Campolongo, F., Cariboni, J., Gatelli, D., Saisana, M. & Tarantola, S. (2007). *Global Sensitivity Analysis. The Primer*, 1st edn, Johhn Wiley & Sons, Chichester, UK. See

https://onlinelibrary.wiley.com/doi/book/10.1002/9780470725184 (accessed 02/10/2023).

Santner, T. J., Williams, B. J. & Notz, W. I. (2018). Sensitivity analysis and variable screening. In *The Design and Analysis of Computer Experiments*. Springer Series in Statistics, Springer, New York, NY, USA, pp. 247–297. See http://link.springer.com/10.1007/978-1-4939-8847-1_7 (accessed 18/08/2023).

Sarsby, R. W. (1985). The design and analysis of computer experiments. In *Proceedings of the Second Canadian Symposium on Geotextiles and Geomembranes*, Canadian Geotechnical Society, Edmonton, AB, Canada, pp. 7–12.

Schwarz, G. (1978). Estimating the dimension of a model. *The Annals of Statistics*, **6**, No. 2, 461–464, https://doi.org/10.1214/aos/1176344136.

Seabold, S. & Perktold, J. (2010). Statsmodels: econometric and statistical modeling with python. In *Proceedings of the 9th Python in Science Conference*, Austin, TX, USA, van der Walt, S. & Millman, J., Editors, pp. 92–96. See https://conference.scipy.org/proceedings/scipy2010/seabold.html (accessed 08/07/2022).

Sieira, A. C. C. F., Gerscovich, D. M. S. & Sayão, A. S. F. J. (2009). Displacement and load transfer mechanisms of geogrids under pullout condition. *Geotextiles and Geomembranes*, **27**, No. 4, 241–253, https://doi.org/10.1016/j.geotexmem.2008.11.012.

Snyman, J. A. & Wilke, D. N. (2018). *Practical Mathematical Optimization*, 2nd edn, Springer International Publishing, Cham, Switzerland. See http://link.springer.com/10.1007/978-3-319-77586-9 (accessed 19/06/2023).

Sobhi, S. & Wu, J. T. H. (1996). An interface pullout formula for extensible sheet reinforcement. *Geosynthetics International*, **3**, No. 5, 565–582, https://doi.org/10.1680/gein.3.0075.

Spearman, C. (1904). The proof and measurement of association between two things. *The American Journal of Psychology*, **15**, No. 1, 72, https://doi.org/10.2307/1412159.

Sugimoto, M. & Alagiyawanna, A. M. N. (2003). Pullout behavior of geogrid by test and numerical analysis. *Journal of Geotechnical and Geoenvironmental Engineering*, **129**, No. 4, 361–371, https://doi.org/10.1061/(ASCE)1090-0241(2003)129:4(361).

Sweta, K. & Hussaini, S. K. K. (2018). Effect of shearing rate on the behavior of geogrid-reinforced railroad ballast under direct shear conditions. *Geotextiles and Geomembranes*, **46**, No. 3, 251–256, https://doi.org/10.1016/j.geotexmem.2017.12.001.

Tavakoli Mehrjardi, G. & Khazaei, M. (2017). Scale effect on the behaviour of geogrid-reinforced soil under repeated loads. *Geotextiles and Geomembranes*, **45**, No. 6, 603–615, https://doi.org/10.1016/j.geotexmem.2017.08.002.

Taylor, R. N. (1995). Centrifuges in modelling: principles and scale effects. In *Geotechnical Centrifuge Technology*, New York, NY, USA, Taylor, R. N., Editor, Blackie Academic & Professional, London, NY, USA, pp. 19–33.

Teixeira, S. H. C. (2003). *A Soil-Geogrid Interaction Study on Pullout Tests and its Application on Analysis and Designing of Reinforced Soil Structures (In Portugese: Estudo da interação solo-geogrelha em testes de arrancamento e a sua aplicação na análise e dimensionamento de maciços reforçados)*, PhD dissertation, University of São Paulo, São Carlos, Brazil. See http://www.teses.usp.br/teses/disponiveis/18/18132/tde-07042006-114840/ (accessed 17/05/2023).

Teixeira, S. H. C., Bueno, B. S. & Zornberg, J. G. (2007). Pullout resistance of individual longitudinal and transverse geogrid ribs. *Journal of Geotechnical and Geoenvironmental Engineering*, **133**, No. 1, 37–50, https://doi.org/10.1061/(asce)1090-0241(2007)133:1(37).

Virtanen, P., Gommers, R., Oliphant, T. E., Haberland, M., Reddy, T., Cournapeau, D., Burovski, E., Peterson, P., Weckesser, W., Bright, J., van der Walt, S. J., Brett, M., Wilson, J., Millman, K. J., Mayorov, N., Nelson, A. R. J., Jones, E., Kern, R., Larson, E., Carey, C. J., Polat, İ., Feng, Y., Moore, E. W., VanderPlas, J., Laxalde, D., Perktold, J., Cimrman, R., Henriksen, I., Quintero, E. A., Harris, C. R., Archibald, A. M., Ribeiro, A. H., Pedregosa, F. & van Mulbregt, P. (2020). Scipy 1.0: fundamental algorithms for scientific computing in python. *Nature Methods*, **17**, 261–272, https://doi.org/10.1038/s41592-019-0686-2.

Wang, J., Liu, F. Y., Zheng, Q. T., Cai, Y. Q. & Gou, C. F. (2021). Effect of aperture ratio on the cyclic shear behaviour of aggregate-geogrid interfaces. *Geosynthetics International*, **28**, No. 2, 158–173, https://doi.org/10.1680/jgein.20.00038.

Willmott, C. J., Robeson, S. M. & Matsuura, K. (2012). A refined index of model performance. *International Journal of Climatology*, **32**, No. 13, 2088–2094, https://doi.org/10.1002/joc.2419.

Wilson-Fahmy, R. F. & Koerner, R. M. (1993). Finite element modelling of soil-geogrid interaction with application to the behavior of geogrids in a pullout loading condition. *Geotextiles and Geomembranes*, **12**, No. 5, 479–501, https://doi.org/10.1016/0266-1144(93)90023-H.

Zhou, J., Chen, J. F., Xue, J. F. & Wang, J. Q. (2012). Micro-mechanism of the interaction between sand and geogrid transverse ribs. *Geosynthetics International*, **19**, No. 6, 426–437, https://doi.org/10.1680/gein.12.00028.

Ziegler, M. & Timmers, V. (2004). A new approach to design geogrid reinforcement. In *Proceedings of the 3rd European Geosynthetics Conference*, Munich, Germany, pp. 661–666.

Zornberg, J. G., Roodi, G. H. & Gupta, R. (2017). Stiffness of soil–geosynthetic composite under small displacements: I. Model development. *Journal of Geotechnical and Geoenvironmental Engineering*, **143**, No. 10, 04017075, https://doi.org/10.1061/(asce)gt.1943-5606.0001768.

The Editor welcomes discussion on all papers published in Geosynthetics International. Please email your contribution to discussion@geosynthetics-international.com by 15 December 2025